Direct Numerical Simulation and Modelling Study of the Structures and Propagation of Partially Premixed Turbulent Flames

Holmen, Vivianne

2015

LUNDS
UNIVERSITET

Direct Numerical Simulation and Modelling Study of the Structures and Propagation of Partially Premixed Turbulent Flames

Vivianne Holmén Notander

Licentiate Thesis

Lund 2015
Division of Fluid Mechanics
Department of Energy Sciences
Lund University

ISRN LUTMDN/TMHP-15/7094-SE
ISSN 0282-1990

Division of Fluid Mechanics
Department of Energy Sciences
Faculty of Engineering
Lund University
Box 118
S-221 00 LUND
Sweden

Typeset in LaTeX
Printed by Tryckeriet i E-huset, Lund, September 2015

Abstract

Turbulent partially premixed flames are found in common combustion applications, such as the lifted jet flames in diesel engines. There is less theory surrounding the structure and propagation of turbulent partially premixed flames than for classical premixed flames and diffusion flames, especially in regards to modelling. This thesis presents direct numerical simulations (DNS) and analysis of the structures and propagation of turbulent partially premixed flames. The aim is to collect detailed information on turbulent partially premixed flames and to provide insight for the development of models for turbulent partially premixed flames.

The fuels considered are methane and hydrogen, with unity Lewis number and Lewis number less than one, respectively. A detailed chemical kinetic mechanism and mixture averaged transport properties were used in the DNS. The computations were carried out at room temperature and atmospheric pressure in a rectangular domain of size of 20 mm, 10 mm and 10 mm in the streamwise and cross flow directions respectively. Isotropic turbulence was imposed at the inflow boundary and the inflow velocity was selected such that the flame was stabilized in the domain during the time span of the simulation. The two simulated flames have similar turbulence conditions. The Karlovitz number of the methane/air flame is about 50 at the triple-point of the flame, and for the hydrogen/air it is about 5. The DNS was carried out using a high order finite difference code.

Both the turbulent methane/air and hydrogen/air partially premixed flames consist of a main premixed flame front trailed by two thin lean premixed flames at the edges and a diffusion flame following the stoichiometry line. The lean premixed flames can be sustained at much lower equivalence ratio than the corresponding planar unstretched laminar premixed flames. The leading front has a w-shaped structure, with weak reactions distributed on the burned side of the premixed flame. Turbulent eddies wrinkle the flames in both cases and broaden the preheat zone. The hydrogen flame is wrinkled at smaller scales than the methane flame, despite having very similar turbulence. The lean trail and the diffusion flame both have a heat release rate roughly two orders of magnitude lower than that of the premixed front.

The propagation of turbulent partially premixed flames are shown to be highly sensitive to local equivalence ratio, curvature and strain rate of the flame, and local turbulent motion. The triple flame enhances the displacement speed of stoichiometric mixture of hydrogen due to the interaction between the diffusion flame and premixed flames. The effect of turbulent eddies is shown to highly disturb the flame structures and local displacement speed, which poses a great challenge to the development of cost-effective CFD models for turbulent partially premixed flames under high Karlovitz numbers.

Descriptors: Partially premixed flames, direct numerical simulation, displacement speed, G-equation, modeling.

Contents

1 Introduction

Turbulent flames are seen in nature as well as in industrial applications; a forest fire is one of the most iconic examples of turbulent flames found in nature. A forest fire is more powerful and difficult to extinguish in very windy weather. Turbulent flames have several advantages over their laminar counterparts and are therefore widely used in energy and power production devices such as gas turbines, internal combustion engines and furnaces. Turbulent flames enable a much faster burning rate of fuel and faster oxidation and for this reason can provide a higher power output within a small combustor.

Turbulent flames can be classified into different types [59]: turbulent diffusion flames, turbulent premixed flames and turbulent partially premixed flames. Turbulent diffusion flames are flames where the fuel and the oxidizer react as they mix; turbulent premixed flames are flames where the fuel and the oxidizer are mixed prior to entering the reactor. A forest fire is an example of turbulent diffusion flames naturally ocurring in nature. Diesel engines, rocket engines and aircraft engines are examples of diffusion flames in engineering applications. Since the fuel and oxidizer are not premixed before entering the reactor there is no risk for uncontrolled ignition of the fuel/air mixture outside the desired reaction zone. This makes diffusion flames advantageous in terms of safety control. The reaction zone in a diffusion flame is located where the fuel and the oxidizer mixture reaches an equivalence ratio of unity, i.e. at stoichiometry. The maximum flame temperatures are found at stoichiometry, which means diffusion flame temperatures are the highest possible for a given fuel. High combustion temperatures favour complete combustion, however, this is at the cost of high NO_X production as NO_X production increases exponentially with temperature increases.

In premixed flames the fuel and the oxidizer are mixed before entering into the combustion zone which makes it possible to control the ratio of fuel to oxidizer in the mixture, thereby controlling combustion temperature. A mixture with a non-unity equivalence ratio will have a lower combustion temperature since the heat released in the chemical reactions is used to heat up the combustion products as well as the remaining fuel and/or oxidiser. The reaction zone of a turbulent premixed flame is not localised – in contrast to the turbulent diffusion flame where the reaction zone is found at stoichimetry – the reaction zone in a turbulent premixed flame propagates in the fuel/oxidizer mixture. Propagating flames are more difficult to work with from a safety point of view as the flame can move around inside the combustor or out of it entirely. When combined with the fact that the mixture is flammable before entering the combustor, it becomes clear that understanding how the flame will propagate is of special interest concerning safety. A practical question is thus how fast a turbulent premixed flame can propagate; this is related to the structure of the flames and turbulence/flame interaction. There is therefore a great amount of current research on turbulent premixed flames [59, 18, 15, 16].

Turbulent partially premixed flames are flames that share common characteristics with both diffusion flames and premixed flames [7]. Part of the flame – the leading front of the flame – propagates as a premixed flame, while another part of the flame – the trail of the flame – burns as a diffusion flame. At first glance, using turbulent partially premixed flames seems to be something that should be avoided – the flames have both the disadvantage of high combus-

tion temperatures with the resulting high NOx production, and the problems associated with a propagating reaction front.

Turbulent partially premixed flames are unfortunately unavoidable in practical applications. A perfect premixed flame cannot always be generated in a combustor. A stratified premixed mixture where the mixture varies from lean to rich in the combustor can form a partially premixed flame. The flame front consists of a rich premixed flame and a lean premixed flame. The fuel in the rich part of the flame is not all burned due to the lack of oxygen; the oxygen in the lean part of the flame is not completely consumed due to the lack of fuel. As a result, the leftover fuel downstream of the rich part of the flame will react with the remaining oxygen from the lean part of the flame, thereby forming a diffusion flame trailing behind the premixed flame. Together, the lean premixed flame, the rich premixed flame and the diffusion flame form a triple-flame whose intersection point (known as the triple point) is found where the equivalence ratio is equal to one. The structure and propagation of turbulent partially premixed flames depend on the local mixture and turbulence conditions.

Partially premixed flames can also be found in combustors meant to work in the diffusion flame mode, for example diesel engines. The liquid fuel is injected through a small nozzle into the cylinder where it needs time to atomize and evaporate. When this has occured, the vapour fuel and air begin mixing until they reach the correct composition. The combustion zone is therefore located at the downstream end of the diesel jet. When the fuel ignites a small premixed flame is formed around the diffusion flame where the fuel/air mixture is flammable but not of unity equivalence ratio, therefore resulting in a partially premixed flame. In diesel engines the triple-flame propagation is one of mechanisms that stabilise the lift-off of the flame and it has a great impact on NOx and soot formation.

Compared to the research on turbulent diffusion flames and turbulent premixed flames, studies on turbulent partially premixed flames are behind. The results of research on partially premixed flames include several controversies. For example, some authors have found that the propagation speed at the triple point in a turbulent partially premixed flame is much higher than that of a stoichiometric premixed flame, while others have found evidence suggesting the opposite. Perhaps unsuprisingly, modelling of turbulent partially premixed flames is a less mature area than its counterparts for turbulent premixed and diffusion flames.

This thesis aims to provide a fundamental study of the structures of turbulent partially premixed flames. The goal is to analyse the different reaction layers and the preheat layer in a turbulent partially premixed flame and to study how the flames propagate. Direct numerical simulation (DNS) data is used to perform the analysis. The scope of the thesis is as follows:

- detailed analysis of the structures of turbulent partially premixed flames;
- exploration of the effect of turbulence on the structures and propagation of partially premixed flames;
- exploration of the effect of differential diffusion on partially premixed flames;
- examination of modelling approaches for turbulent partially premixed flames.

This thesis is arranged as follows: In Chapter 2 a survey of the existing literature for partially premixed flames is presented, including laminar partially premixed flames and modelling of partially premixed flames. In Chapter 3 the direct numerical simulation methods are presented. The main results are discussed in Chapter 4, followed by a summary of the main conclusions of this thesis and future work in Chapter 5.

2 Literature Review and Research Questions

In order to provide the definition of partially premixed flames there are several basic concepts that need to be clarified first. When discussing combustion it is common to use the words *flame* and *combustion* interchangeably. Combustion is the term applied to all types of exothermic chemical reactions where a fuel is oxidised. Combustion can refer to both rapid chemical reactions and slow ones, from an engineering point of view only the rapid reactions are of interest. Combustion can occur in flame or non-flame mode. The different modes of combustion have different characteristics and must therefore be distinguished with care.

- **Flames** - A flame is a specific mode of combustion where intense chemical reaction occurs in thin layers. The flame mode is most common for applications of combustion. Flames can be of three different types: premixed, non-premixed and partially premixed. The terminology refers to whether the fuel is mixed with oxidiser before ignition or not. Partially premixed flames are a combination of the two ideal scenarios, showing characteristics of both types of flames. In addition, flames can be turbulent or laminar, depending on the characteristics of the flow. Turbulence can change the structure of the flame. Flame propagation is refered to as deflagration.
- **Ignition Waves** - This is a combustion mode belonging to the the non-flame group. An ignition wave can behave similarly to a propagating flame. It is however fundamentally different as it is not constrained by a flame speed and is in fact a mixture of fuel and oxidiser autoigniting. Autoignition is the term used when rapid oxidation reactions occur at many locations within the unburned gas, leading to a very rapid combustion throughout the volume, with an essentially volumetric heat release [83]. The propagation speed of an ignition wave is a function of the local mixture's ignition delay time and the gradient of temperature, composition, and pressure [96, 21, 17, 97]. Homogeneous charge compression ignition (HCCI) engine combustion is typically governed by the propagation of ignition waves [19, 89].
- **Detonation Waves** - As opposed to deflagration waves, which refers to premixed flames, detonation is a mode of combustion involving a supersonic exothermic front accelerating through a medium that eventually drives a shock front propagating directly in front of it [85].

This thesis is devoted to the study of partially premixed flames; thus we will not go into further detail regarding the latter two modes of combustion.

2.1 Partially Premixed Flame Structure

Since a partially premixed flame consists of both a premixed flame (with stratification of fuel in the fuel/air mixture) and a diffusion flame, we will provide a theoretical background of both flame modes.

2.1.1 Mixture fraction and scalar dissipation rate

In a non-premixed flame the reactions are assumed to occur very rapidly in a thin layer at stoichiometric fuel/air ratio. The fuel and the oxidiser first come into contact with each other inside the combustor, which means the process of mixing both components is responsible for the position of the flame. This is why non-premixed flames are often called *diffusion flames*. Hence, the structure of a non-premixed flame is dependent on both the mixing process and the chemical reactions [60, 74, 74, 3].

The mixing process in turbulent flow is very complex, especially when combustion is taken into account, as it adds heat realease, varying densities and volumentric expansion into the problem. However, if all species can be said to mix in the same way, a single variable would suffice to compute the mixing of the different elements. Therefore, assuming the diffusion coefficients of all scalars are equal the mixing process can then be described by generating a scalar called the *mixture fraction*, Z. Mixture fraction can be defined in different ways [83, 6]. A simple definition for cases when the fuel and oxidiser are segregated into separate streams is the ratio of mass originated from the fuel stream to the total mass in the mixture [22].

A transport equation for mixture fraction can be derived from the transport equations of species. The equation can be written as follows in a Cartesian coordinate system where velocity in the x_i direction is denoted by u_i, the density of the mixture by ρ and the diffusion coefficient of the mixture D,

$$\rho\frac{\partial Z}{\partial t} + \rho u_i \frac{\partial Z}{\partial x_i} = \frac{\partial}{\partial x_i}\left(\rho D \frac{\partial Z}{\partial x_i}\right) \tag{1}$$

An assumption underlying this definition of mixture fraction is unity Lewis number. The Lewis number, defined as $Le = \lambda/\rho c_p D$, where λ is the thermal conductivity, ρ is the density, c_p is the heat capacity at constant pressure and D is the diffusion coefficient, is the ratio between thermal diffusivity and mass diffusivity of the mixture. The assumption of unity Lewis number means that energy is assumed to diffuse at the same rate for all species.

The unity Lewis number assumption works well for methane flames for example, where all the major species have a Lewis number close to unity, therefore Eq. (1) is a good model for such flames. However, large hydrocarbons and hydrogen have Lewis numbers that significantly differ from one, making this assumption less accurate. The result of varying Lewis numbers is that temperature and species will diffuse in opposite directions when gradients are present. This effect is known as differential diffusion. As Eq. (1) does not consider the effects of differential diffusion a more detailed transport equation for mixture fraction has been developed by Pitsch and Peter [62] to account for this.

Eq. (1) is sufficient to compute mixture fraction in several practical application and the model has proven to be very useful [1, 63]. However, it is important to be aware of the simplification made and the effect they have on the physical interpretation of mixture fraction.

Using Eq. (1) to analyse a stationary jet flame with jet velocity U and jet radius R, one can see that the convection term is of the order of $\rho U/L_f$, while the diffusion term is of the order of $\rho D/R^2$. Balancing these two terms one can see that the length of the flame L_f is determined by the jet velocity, jet radius, and diffusion coefficient:

$$L_f \sim UR^2/D \tag{2}$$

In turbulent flames turbulent eddy motion dominates the mixing process. The diffusion coefficient D in Eq. (2) is therefore replaced by the turbulent eddy viscosity.

There is no term providing information about the chemical reactions in Eq. (2), this means that the shape and length of the flame can be fully described by the characteristics of the flow and mixing. However, the reaction zone structure of a diffusion flame is not only governed by the mixing process. It is also affected by chemical reactions. Specifically, it is governed by the competition between the mixing rate and the chemical reaction rate. The mixing rate can be described by the *scalar dissipation rate*, χ, defined as

$$\chi = 2D\frac{\partial Z}{\partial x_i}\frac{\partial Z}{\partial x_i} \tag{3}$$

The ratio between the chemical reaction rate and mixing rate is often referred to as the Damkohler number, Da,

$$Da = \dot{\omega}/\chi \tag{4}$$

It determines whether the flame structure will be dominated by chemical reaction or by the mixing process. When the scalar dissipation rate is lower than the chemical reaction rate there is sufficient time to complete the oxidation of the fuel, which gives rise to a high flame temperature. The high flame temperature further increases the chemical reaction rate. Combustion with low scalar dissipation rate therefore favours complete combustion. On the other hand if the scalar dissipation rate is too high, the chemical reaction may be unable to keep up, leading to quenching.

Eq. (3) shows that high scalar dissipation rates are found where the gradient of mixture fraction is high. In a jet flame the gradient is the highest near the nozzle. This is the region where the flame can be quenched.

If the mixture is not ignited by this point the fuel and air will continue to mix. The fuel/air mixture can then be ignited by an external source of heat, e.g. the spark in a cigarette lighter. Due to the prolonged mixing there will now be regions of flammable non-stoichiometric mixture surrounding the area where the mixture has reached stoichiometry. This means that combustion for such a case, where the chemical reactions occur downstream of the fuel jet nozzle, is in fact in the partially premixed flame mode. In a partially premixed flame, the mixture fraction model is no longer sufficient to describe the combustion as the physics of such a flame differ substantially from the non-premixed case.

Figure 1 shows the structure of a partially premixed flame. A partially premixed flame is made up of a lean premixed flame, a rich premixed flame and a diffusion flame. The diffusion flame forms a trail starting the mixture is stoichiometric ($\Phi = 1$). A premixed flame front is found ahead of the diffusion flame, therefore it is called the leading front. The diffusion flame intersects with the premixed flames at the triple-point. The relative size of the diffusion trail versus the premixed front varies depending on the application, meaning a partially premixed flame may be dominated by either a non-premixed flame or a premixed flame. It is sometimes assumed that a partially premixed flame can be separated into purely non-premixed parts and purely premixed ones instead

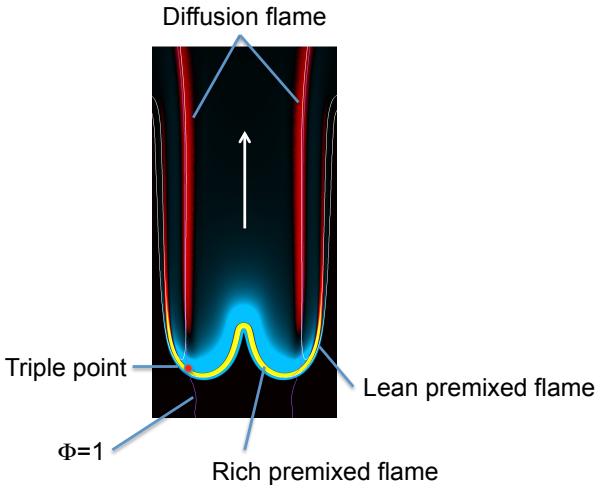

Figure 1: The reaction zone structure of a partially premixed methane/air flame. Detailed discussion of this figure is given in Section 4.

of being considered a flame mode in itself. In the next section premixed flames are discussed.

2.1.2 Structures and propagation of leading premixed flame fronts

A general description of premixed combustion requires an explanation of the mechanism of flame propagation. In a flammable mixture of fuel and air a flame can be initiated by an external heat source. Once ignited the flame will release heat that is diffused to the low temperature zone, i.e. the unburned gases. The hot combustion products also diffuse from the flame. The rate of heat diffusion is proportional to the diffusion coefficient of heat, as well as to the gradient of temperature. The diffusion of heat warms up the surrounding unburned gases until they reach a certain temperature, the *ignition temperature*, T_0. At this temperature the fuel/air mixture will ignite. Once the flame has been initiated the flame is self-sustained by using up the unburned mixture. This diffusion-reaction process results in a reaction zone that is progressively moving toward the unburned mixture. This is what is referred to as the *propagation of a premixed flame*, the flame speed often denoted by S_L.

Studies on the structure and propagation of premixed flames can be traced back to the work of Le Chatelier and Mallard [48]. The basic structure of a premixed flame can be described using a three-layer model. As shown in Figure 2 The flame consists of a preheat layer, a reaction layer and a post-flame zone. The preheat layer has a thickness of δ_H and consists of the zone where the unburned gases have been heated and some low temperature intermediate species can be found. The reaction layer, with a thickness of δ_R, is where the heat is released and the fuel is consumed. The thick post-flame layer consists of combustion products at high temperature downstream the reaction layer.

In order to derive relationships for the flame speed and thickness one can look at the governing equation of temperature. It can be simplified as follows,

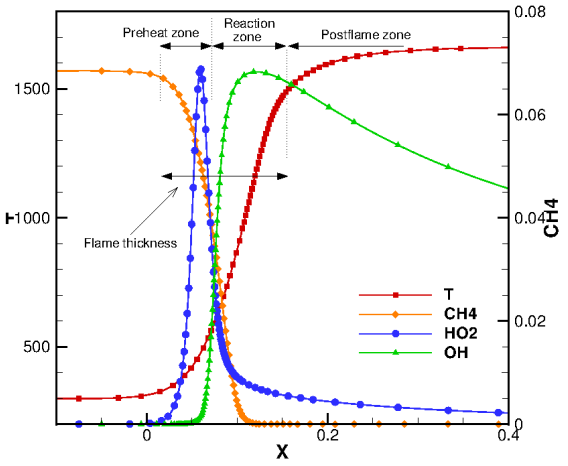

Figure 2: The flame structure of a 1D planar premixed flame. OH is used as an indicator of reaction zone in this example.

$$\rho \frac{\partial \theta}{\partial t} + \rho u_i \frac{\partial \theta}{\partial x_i} = \frac{\partial}{\partial x_i} \left(\rho \alpha \frac{\partial \theta}{\partial x_i} \right) + \rho \dot{\omega}_\theta \tag{5}$$

where α is the diffusion coefficient of heat, $\dot{\omega}_\theta$ is rate of heat release. Here, θ is normalized temperature,

$$\theta = \frac{T - T_u}{T_b - T_u} \tag{6}$$

where T_u and T_b are the temperatures of the unburned and burned mixtures respectively. The mixture fraction cannot be used for premixed combustion. If the mixture has a uniform equivalence ratio the mixture fraction is also uniform everywhere, regardless of whether it is in the burned or unburned side of the flame. In premixed combustion the flame is usually identified using a reaction progress variable instead. This is a variable that varies between 0 and 1 depending on the progress of the chemical reactions. As θ varies between 0 in the unburned mixture and 1 in the burned mixture it can be used as a reaction progress variable.

In order to derive relations for the flame speed, S_L, and flame thickness, δ_L, we consider a one-dimensional planar premixed flame propagating in a homogeneous fuel/air mixture without convective flow motion. Setting the convection flow motion to zero means that in a coordinate fixed at the flame front, the unburned fuel/air mixture moves towards the flame at a velocity of S_L, that is u_i is equal to S_L in Eq. 5. The flame thickness is assumed to be the layer where temperature changes form T_u to T_b, that is $\delta = 1/d\theta/dx$. By then looking at the flame in the preheat and reaction layers separately the following relations can be obtained:

In the preheat zone there is no heat release and temperature does not change over time, therefore only the convection and diffusion terms remain in Eq. (5), therefore across the preheat zone,

$$\rho S_L/\delta_L \sim \rho\alpha/\delta_L^2 \tag{7}$$

In the reaction zone heat release rate is the dominant term. It is balanced by the heat diffusion term,

$$\rho\dot{\omega}_\theta \sim \rho\alpha/\delta_L^2 \tag{8}$$

Combining Eqs.(7) and (8) it can be shown that

$$S_L \sim \sqrt{\alpha\dot{\omega}_\theta} \tag{9}$$

and

$$\delta_L \sim \sqrt{\alpha/\dot{\omega}_\theta} \tag{10}$$

Eq. (9) states that flame propagation is proportional to heat release rate and the thermal diffusion coefficient. This is not surprising, as high heat release will increase chemical reaction rates and a high thermal diffusion means that the unburned gases will reach ignition temperature faster. From Eq. (10) it can be seen that high heat release rate results in a thin flame. In combustion of practical fuels the flame thickness is typically less than one millimeter [45]. It is worth noting that according to Eqs. (9,10) premixed flame propagation is independent of the velocity of the flow.

Several more detailed analysis of the flame structure and propagation of premixed flame speeds have been developed by a variety of researchers. Different assumptions are made in order to study specific characteristics. For example Zel'dovich has models based on one-step chemistry and high activation energy asymptotics [95]. There are also a number of models based on multiple-step chemistry and rate-ratio asymptotics [73, 72, 70, 71].

In the above discussion the flame has been assumed to be planar and flame area is not a function of time. In general, the flame front can be curved and strained. In this situation S_L is affected by not only the chemical reactions and thermodynamic properties, but also by curvature and strain, that is how the flame is stretched. Following an asymptotic analysis as presented in [59] the flame speed under stretch (curved and strained) can be written as follows,

$$S_L = S_L^0\left[1 - \mathscr{L}\kappa + \frac{\mathscr{L}}{S_L^0}\zeta\right] \tag{11}$$

where $\mathscr{L}$ is the Markstein length, S_L^0 is the laminar burning velocity corresponding to a planar flame, κ is the curvature and ζ the strain.

2.1.3 Propagation of a premixed flame front in a complex flow field

In the previous discussion the unburned mixture has been assumed to have zero velocity. In a complex flow field the flame front position is affected by both the local flow velocity and the propagation speed of the flame. We consider an iso-surface of $\theta = c$, for a value of c within either the preheat zone or the

reaction zone, i.e. $0 < c < 1$. The iso-surface of $\theta = c$ can be discribed by the following function,

$$G(x,y,z,t) = \theta - c = 0 \tag{12}$$

In premixed combustion the flame front is considered to be the chosen iso-surface. The flame front propagates towards the unburned mixture with a local displacement speed S_d in a flow field with velocity $\bar{v}$. The displacement speed is defined such that the convection of the fluid is not included, but only the self-propagation is taken into account. A point on the flame front can be denoted as

$$\bar{r_p} = x\bar{e_x} + y\bar{e_y} + z\bar{e_z} \tag{13}$$

The motion of each point $\bar{r_p}$ is governed by the following equation

$$\frac{\bar{r}_p}{dt} = \bar{v} + S_d\bar{n} \tag{14}$$

In this equation $\bar{n}$ is the direction normal to the flame surface.

The level set framework, which will be described in section 2.3, provides a convenient way to describe the theory of propagation speed. A level set is the set of points with the same value, Eq. (12) is therefore the zero-level set. A time derivative of the level set G

$$\begin{aligned} \frac{dG}{dt} &= \frac{\partial G}{\partial t} + \frac{\partial G}{\partial x}\frac{\partial x}{\partial t} + \frac{\partial G}{\partial y}\frac{\partial y}{\partial t} + \frac{\partial G}{\partial z}\frac{\partial z}{\partial t} && (15)\\ &= \frac{\partial G}{\partial t} + \nabla G\frac{d\bar{r_p}}{dt} && (16)\\ &= 0 && (17) \end{aligned}$$

and combining this with the description of the motion of each point we get

$$\frac{\partial G}{\partial t} + \nabla G \cdot (\bar{v} + S_d\bar{n}) = 0 \tag{18}$$

which, using $\bar{n} = -\nabla G/|\nabla G|$ results in what is commonly referred to as the G-equation.

$$\frac{\partial G}{\partial t} + \bar{v} \cdot \nabla G = S_d|\nabla G| \tag{19}$$

It is important to note that this derivation is only valid for points inside the set $G(x,y,z,t) = 0$,, i.e. for points on the flame surface. The equation lacks physical meaning outside this surface. In combustion the G-equation is commonly referred to as the level-set equation. The G-equation is a first order Hamilton-Jacobi equation; i.e. a first-order non-linear partial differential equation of the form

$$H + \frac{\partial S}{\partial t} = 0 \tag{20}$$

where H is a function given in the domain known as the Hamiltonian. The Hamiltonian depends on the spatial variables, the function S and the gradient

of S. Equations of this type are known to not have classical solutions in general, therefore the theory of viscosity solutions is necessary for generalised global solutions [20]. As the level.set approach is important in a lot of flame modelling section 2.3 will provide a detailed account of the G-equation.

Substituting G in Eq (12) with $\theta = G + c$ as formulated in Eq. (19) results in a formulation based on a progress variable, therefore presenting a natural connection to the chemical reaction progress of the combustion.

$$\frac{\partial \theta}{\partial t} + \bar{v} \cdot \nabla \theta = S_d |\nabla \theta| \tag{21}$$

Eq. (21) can be introduced to Eq. (5) resulting in the following

$$\rho S_d |\nabla \theta| = \frac{\partial}{\partial x_i} \left(\rho \alpha \frac{\partial \theta}{\partial x_i} \right) + \rho \dot{\omega}_\theta \tag{22}$$

which can be used to compute the local displacement speed of the iso-surface $\theta = c$,

$$S_d = \left(\frac{\partial}{\partial x_i} \left(\rho \alpha \frac{\partial \theta}{\partial x_i} \right) + \rho \dot{\omega}_\theta \right) / \left(\rho |\nabla \theta| \right) \tag{23}$$

Consider a planar flame propagating at constant speed S_L in a flow field where the inflow velocity is set to $v_u = S_L$. The flame will be stabilized at a fixed position. The mass flux across the preheat zone and the reaction zone remains constant due to mass conservation:

$$\rho v = \rho_u v_u \tag{24}$$

where the subscript u is used to denote the unburned mixture. Since the flame is stabilized at a given position, the local displacement speed S_d must be equal to the local flow velocity v, thus

$$\rho S_d = \rho_u S_{d,u} \tag{25}$$

Substituting Eq. (25) into Eq. (23) provides and expression for the displacement speed in terms of the progress variable θ

$$S_{d,u} = \left(\frac{\partial}{\partial x_i} \left(\rho \alpha \frac{\partial \theta}{\partial x_i} \right) + \rho \dot{\omega}_\theta \right) / \left(\rho_u |\nabla \theta| \right) \tag{26}$$

$S_{d,u}$ is the displacement speed of the boundary between the preheat zone and the unburned mixture. It corresponds to the flame speed discussed in the previous section 2.1.2, S_L. For premixed flames where the equivalence ratio is not constant the thickness of the flame varies. The fuel/air mixture in a complex flow field may not have a uniform equivalence ratio, especially if the fuel does not have a unity Lewis number. The flame thickness then will also vary in time. $S_{d,u}$ is in this case very sensitive to where the iso-surface of θ is defined.

2.2 Turbulence/flame interaction in turbulent partially premixed flames

Most partially premixed flames in engineering applications are turbulent flames since the fuel/air velocity in typical combustion devices is high enough such that

the flow become turbulent. Turbulence is a flow state that has several distinct characteristics [82], for example, its wide spectrum of three dimensional eddies, its enhanced mixing rate, and its random nature. Turbulence has a significant effect on partially premixed flames. Flames can also affect the turbulence field. Some aspects of turbulence/flame interaction can be listed as the following:

- Turbulence enhances the mixing of the fuel and oxidizer in the trail diffusion flame and the transfer of heat and combustion products to the unburned mixture in front of the leading premixed flame.
- Turbulence eddies wrinkle the flame front, giving rise to increased flame surface area that can speed up the combustion process in both the leading premixed flame and the trailing diffusion flame.
- Turbulence can quench the flame if the mixing rate (scalar dissipation rate) is too high.
- The flame can also affect the turbulence field. The dilation effect of heat release can suppress the turbulence level by reducing the vorticity of the eddies; the higher viscosity can enhance the dissipation of turbulence and can increase the smallest scale of turbulence, the Kolmogorov scale; the high velocity gradient due to heat release can enhance the production of turbulence.

2.2.1 Turbulent mixing and its effect on the trailing non-premixed flame

The mixing process in a turbulent flow can be explained using the energy cascade theory [66, 36]. A short overview of the energy cascade theory is presented here.

The eddies present in a turbulent flow have a wide range of sizes, the largest one is called the integral scale. In a combustor, the velocity (u_0'), time (t_0) and length (ℓ_0) of the largest eddies is determined by the flow velocity of the fuel/oxidiser streams and the geometry of the combustor itself. The smallest scale of eddies, the Kolmogorov scale, depends on the dissipation rate of turbulent kinetic energy and the viscosity of the fluid.

According to the energy cascade theory, the dissipation rate is constant for all scales. The order of magnitude of the dissipation rate at the Kolmogorov scale, ϵ, is given by

$$\epsilon \sim \nu u_k'^2/\ell_k^2,$$

where ν is the kinematic viscosity of the mixture. The subscript k denotes eddies at the Kolmogorov scale.

The Reynolds number for eddies at the Kolmogorov scale is of the order of one,

$$Re_k \sim u_k' \ell_k/\nu \sim 1.$$

From the previous equations the following relation can be derived

$$u_k' \sim (\nu\epsilon)^{1/4}, \ell_k \sim \left(\nu^3/\epsilon\right)^{1/4}. \tag{27}$$

If the same thing is done for the integral scale we find that the dissipation rate is

$$\epsilon \sim u_0'^3/\ell_0.$$

The Reynolds number for eddies of integral scale is

$$Re_0 \sim u_0' \ell_0 / \nu \gg 1.$$

Through simple mathematical manipulation combining the expressions for the Kolmogorov scale and the integral scale one finds that

$$u_k'/u_0' \sim (t_k/t_0)^{1/2} \sim (\ell_k/\ell_0)^{1/3} \sim Re_0^{-1/4}. \tag{28}$$

where the time scales on the integral scale and Kolmogorov scale are defined as

$$t_0 \sim \ell_0/u_0', t_k \sim \ell_k/u_k'.$$

t_0 and t_k are often referred to as the turnover time of the corresponding eddies. The turnover time is related to the rotation of the eddies.

Equation (28) implies that a high Reynolds number on the integral scale Re_0 corresponds to smaller Kolmogorov scales, with short Kolmogorov eddy turnover times, and lower Kolmogorov eddy velocitie.

The mixing process of the fuel and oxidizer can be understood as follows.

The fuel and oxidiser are brought into contact with each other by the larger eddies. These eddies are moving at a speed of u_0' across a length ℓ_0, which takes the time of t_0. As a result of large eddy breakup there are smaller eddies in the large ones, including the Kolmogorov eddies. The smaller eddies interact in the same way as the large ones, bringing the fuel and oxidiser together, during a shorter time and across a shorter length. On the Kolmogorov scale the mixing process is completed on a the molecular lever, which means the molecular diffusion time is the key to mixing.

The molecular mixing time of the Kolmogorov eddies is

$$t_{k,m} \sim \ell_k^2/\nu,$$

which can be shown to be the same as the eddy time scale for Kolmogorov eddies t_k. This means that the fuel and oxidiser mix on the molecular level within the Kolmogorov eddy turnover time, therefore resulting in the mixing of the two streams.

The turbulent mixing process is controlled by the integral scale eddy turnover time as this is the slowest process of the mixing cascade. The mixing rate can therefore be given as the inverse of the eddy turnover time on the integral scale. If turbulent kinetic energy is denoted by k the mixing rate of fuel and oxidiser in turbulent flow is given by

$$\dot{m} \sim 1/t_0 \sim \epsilon/k, k \sim {u_0'}^2. \tag{29}$$

Introducing the turbulent eddy viscosity in analogy to the molecular mixing process presented before the following relation can be set up

$$\epsilon \sim \nu \left(u_k'/\ell_k\right)^2 \sim \nu_t \left(u_0'/\ell_0\right)^2,$$

which yields

$$\nu_t \sim u_0' \ell_0 \sim k^2/\epsilon.$$

The scalar dissipation rate in the diffusion flame trail of a turbulent partially premixed flame is proportional to $\dot{m}$ [43],

$$\chi \sim \overline{Z'^2}\epsilon/k, \tag{30}$$

where $\overline{Z'^2}$ is the variance of mixture fraction.

Following a similar analysis to that for determining the flame length for a jet in Section 2.1.1, the molecular diffusion coefficient can be replaced by the turbulent eddy diffusion coefficient, resulting in the length of a turbulent jet flame as

$$L_f \sim UR^2/D_t \sim UR^2/\nu_t \sim R\frac{U}{u_0'}\frac{R}{\ell_0}. \tag{31}$$

In a turbulent jet flame the large eddy velocity is proportional to the jet velocity and the large eddy length scale is proportional to the jet radius. The ratios U/u_0' and R/ℓ_0 are fairly independent of U and R. Thus, the length of the turbulent non-premixed flame trail is nearly independent of jet velocity, and consequently also independent of turbulent kinetic energy. This implies that jet velocity and mixing rate are nearly proportional to each other, so if the velocity is increased the mixing rate increases by almost the same factor. This means that the flame length does not need to change in order to accommodate the extra inflow of fuel. This is an important characteristic of diffusion flames since it entails that a combustion device can be run at different loads without a significant change of the flame volume, thus allowing combustor size to remain constant.

When the mixing rate is too high, i.e. the scalar dissipation rate is above a critical value [58, 43, 2], the flame can be locally or globally quenched. Local extinction near the jet nozzle leads to a lifted flame, which can develop into a partially premixed flame depending on the ambient conditions [24].

2.2.2 Eddy/flame interaction and regimes of turbulent premixed flames

At the leading premixed flame front of a turbulent partially premixed flame the eddies interact with the flame in two different ways: First, turbulent eddies can enhance the mixing of hot combustion products with the unburned mixture therefore aiding in the transfer of heat. Second, turbulent eddies wrinkle the flame front, this can significantly increase the flame surface area from that of the corresponding laminar flames. Both of these effects can increase the burning rate and thereby enhance the propagation speed of the flame. The relative importance of these two processes of flame/turbulence interaction can be determined through scale analysis.

The rate of heat transfer between the reaction zone and the preheat zone through molecular diffusion can be estimated as follows,

$$\dot{\theta}_L \sim \alpha/\delta_L^2 \sim S_L/\delta_L.$$

The diffusion rate of heat due to turbulent eddies can be estimated, based on the analysis in the previous section, through the following expression

$$\dot{\theta}_t \sim \epsilon/k \sim u_0'/\ell_0.$$

The ratio of these two is

$$\dot{\theta}_t/\dot{\theta}_L \sim (u_0'/S_L)\,(\delta_L/\ell_0)\,. \tag{32}$$

The physical meaning of Eq. (32) can be explained by looking at several non-dimensional parameters.

The Damkohler number, introduced earlier in this section as the ratio between the chemical reaction rate and the mixing rate, is more specifically the ratio between turbulent large eddy time t_0 and the chemical reaction time $t_c \sim \delta_L/S_L$,

$$Da = t_0/\left(\delta_L/S_L\right).$$

From this definition it becomes clear that $\dot{\theta}_t/\dot{\theta}_L \sim 1/Da$. For flames with large Damkohler numbers, $Da > 1$, the heat transferred through molecular motion between the reaction and the preheat zone is larger than that related to turbulent eddy motion. As molecular motion is the dominating mechanism of heat transfer, meaning the effect of turbulence is not very pronounced, the structure of such flames is similar to that of laminar ones.

In order to more thoroughly discuss the effect of turbulence on the flame structure another non-dimensional variable is introduced: the Karlovitz number. It is defined as the ratio between the chemical reaction time and the Kolmogorov time scale,

$$Ka = \left(\delta_L/S_L\right)/t_k.$$

Using the scale relation discussed in the previous section one can show that

$$Ka = \left(\delta_L/S_L\right)/t_k \sim \frac{\delta_L}{S_L}\frac{u'_k}{\ell_k} \sim \frac{\delta_L^2}{\ell_k^2}\frac{u'_k\ell_k}{S_L\delta_L} \sim \frac{\delta_L^2}{\ell_k^2}. \tag{33}$$

where the relation $S_L\delta_L \sim \alpha \sim \nu$ is used. The Karlovitz number and Damkohler number can be related each other through,

$$Ka = \left(\delta_L/S_L\right)/t_k \sim \frac{\delta_L}{S_L t_0}\frac{t_0}{t_k} \sim \frac{Re_0^{1/2}}{Da}. \tag{34}$$

As the level of turbulence will affect the flame structure it can be useful to separate turbulent premixed combustion into different regimes. Within each regime the flames are expected to be similar, which means that usefulness of specific models and theories will not necessarily be possible to generalise across regimes. Ka and Da can be used to classify 4 different regimes of turbulent premixed combustion:

- $Ka \leq 1$. From Eq. (33) it can be seen that when $Ka \leq 1$, the flame thickness is smaller than the length scale of the Kolmogorov eddies, i.e. $\delta_L \leq \ell_k$. This means that the turbulent eddies cannot enter the preheat and reaction zones. The small scale eddies are also rapidly dissipated into heat, further limiting the effect they could have on the internal flame structure. Note that according to Eq. (34) when $Ka \leq 1$, Da must be greater than one since Re_0 is much greater than one in a turbulent flame. Eq. (32) shows that heat transfer from the reaction to the preheat zone occurs primarily through molecular diffusion. As mentioned earlier, this means that the flame structure is not altered by turbulence and is similar to that of a laminar flame. This regime is therefore referred to as the *laminar flamelet regime* [8, 85, 59]. In this regime turbulence only has a significant effect on the flame wrinkling.

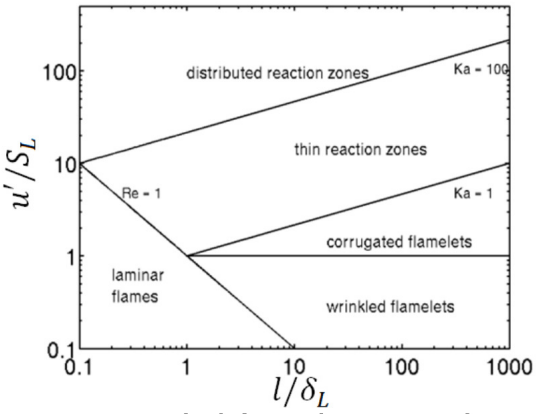

Figure 3: Borghi diagram showing the boundaries to the different turbulent premixed combustion regimes.

- $Da \leq 1$. In this regime $Ka \gg 1$ (cf. Eq. 34). The thickness of the flame is much larger than the Kolmogorov scale. The heat transfer between the reaction zone and the preheat zone is controlled by turbulent eddies (cf. Eq. 32). This regime is referred to as the *distributed reaction zone regime* [8, 85, 59]. Since the eddies can enter the flame in this regime the structures of the preheat and the reaction zones are significantly different from those of laminar flames.

- $Da \geq 1$ and $Ka \geq 1$. In this regime the heat transfer from the reaction to the preheat zone is governed by molecular motion but it can also be affected by turbulent eddy transfer. Peters [59] showed that when $Da \geq 1$ and $1 \leq Ka \leq 100$ the thin fuel consumption zone of a hydrocarbon flame is similar to that of laminar flamelet. However, the preheat zone is broadened, hence small turbulent eddies can enter it. This regime of combustion is referred to as the *thin-reaction zone regime*.

The regimes can be clearly shown in the Borghi diagram, Figure 3. The cases presented in this work are found in the thin reaction zone regime and the distributed reaction zones regime, which may not allow for flamelet models to be used.

2.3 Modelling of turbulent partially premixed flames

As discussed in the previous sections turbulent partially premixed flames are made up of a leading premixed flame with fuel/oxidizer mixture of non-uniform equivalence ratio, followed by a trailing diffusion flame. This complicated flame structure poses a great challenge to modelling and CFD simulations [7]. While a vast literature exists for the modelling of premixed flames and diffusion flames, for partially premixed flames the literature is rather limited.

In principle, models developed for premixed flames and diffusion flames can be combined together to work as the model for partially premixed flames. General models developed that have been developed to work for combustion in

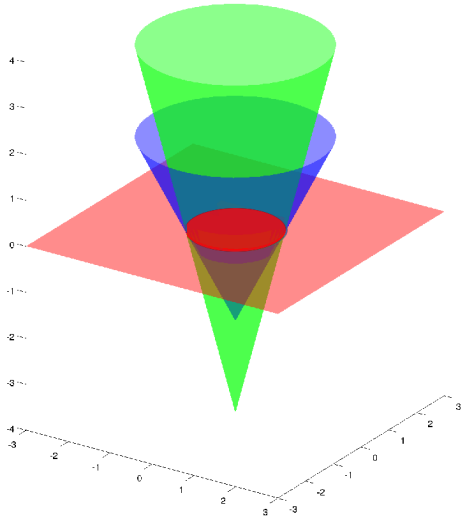

Figure 4: An illustration of the relation between the surface and its zero-level set.

all modes, e.g., finite-rate chemistry models [47, 37, 68, 30, 79], the probability density function based models [65, 26], can be used for partially premixed flames. However, mode-specific models are usually more efficient and are for this reason used more frequently in engineering applications. In this thesis we examine two types of mode-specific models, namely the reaction progress variable/mixture fraction model [9] and the G-equation/mixture fraction model [52, 50, 51, 13, 14, 40]. In both these models the premixed flame front is described using either the reaction progress variable or the level-set G-equation, and the trailing diffusion flame is modelled using mixture fraction and scalar dissipation rate.

2.3.1 The level-set approach for the premixed flame front

The main idea of the level set method is to embed an interface into a scalar field. This scalar field can geometrically be seen as a surface of one more dimension than that of the original interface, i.e. for a 2D curve the level set approach will evolve a 3D surface instead. The surface is linked to the evolution equation as an initial value problem, by building a surface with its zero level set equal to the initial position of the interface, in the context of combustion the interface is set to the flame front. For example, if a 2D circle is to be studied, a cone can be constructed as 3D surface as long as the intersection between the zero-plane and the cone coincides with the 2D circle, see Figure 4.

This method has advantages when dealing with the topology of the surface. The level set approach also makes it simple to determine geometrical properties of the front, such as curvature and normal direction. The theory of viscosity solutions of partial differential equations guarantees a unique weak solution to the equation. From a numerical point of view, this method allows for the use of

accurate schemes developed for the solution of hyperbolic conservation laws.

The level set method can also aid in avoiding problems that arise in combustion modelling due to the sharp change of density, ρ, and viscosity, μ, that occurs at the flame front as a result of temperature increase and the change in composition of the mixture.

From Figure 4 it can be seen that several surfaces can be fitted to the initial interface, in fact there is an infinite number of surfaces that can be constructed for any given interface. The choice of a smooth surface (a surface that has no discontinuities) is preferable to maintain the gradients bounded in the numerical solution [75].

The main problem of the method arises because the evolution equation is only valid at the interface itself, related to combustion this is consistent with the physical behaviour as only the flame has a propagation speed. In addition to the propagation speed, combustion applications have the underlying velocity set to the flow velocity in the whole domain. As the flow velocity is not necessarily uniform advancing, the surface with this velocity is likely to deform the surface which can lead to a loss of smoothness [75]. A loss of smoothness poses numerical problems. The gradients at the discontinuities become unbounded, which can cause the numerical solution to become unstable.

Relation to the signed distance function

As mentioned, the only formal requirement for choosing the surface in the level set method is that its zero-level set coincides with the interface in the original problem. However, some choices of surface result in a simplification of the problem. For this reason, a common choice is to use the signed distance function of the interface as its 3D surface.

A signed distance function (SDF) is a distance function defined as positive on one side of the interface and negative on the other. The boundary separating two regions is considered to be a part of one of the sets.

$$\Phi(x) = \begin{cases} d(x,S^c), x \in S \\ -d(x,S), x \in S^c \end{cases} \qquad d(x,S) = \inf_{y \in S} d(x,y) \tag{35}$$

The distance function $d(x,y)$ can be defined in any metric, most commonly Euclidean. A property of a distance function is that the magnitude of the gradient is identical to one almost everywhere.

$$|\Phi| = 1 \tag{36}$$

This is known as the Eikonal equation. It is true everywhere except where the gradient is undefined, for example the SDF of a circle is a cone with a slope equal to one everywhere except for at the tip.

Having a gradient identical to one makes this interesting for numerical applications where simplifications can be introduced if the magnitude of the normal is equal to one. For this reason especially, the level set method is generally implemented as a signed distance function. By adding the requirement that the surface be a signed distance function of the interface a limit is imposed to how many possible surfaces can be chosen for a given problem.

However, while the advantages of having a smooth bounded surface are many, several difficulties arise when using an SDF as a scalar field to describe an interface that evolves following a Hamilton-Jacobi equation, which as mentioned before in Section 2.1.3 the level set equation is. The main difficulties are described in the list below.

- **SDFs are not solutions to Hamilton-Jacobi equations.** This means that the solution each time-step will not have a gradient of magnitude one, except in special cases. [23]
- **Using the Eikonal equation as a constraint.** When the solution of the evolution equation does not conform to $|\Phi| = 1$ forcing the surface to be an SDF can disturb the position of the zero level set. [67]
- **Determining the distance to the interface.** In a discretised domain the interface is smaller than the smallest grid as the interface is an infinitely thin boundary. This means that the distances themselves cannot be uniquely determined as the exact position of the interface in a subgrid level is not known. [80]

There are different approaches to solving some of the problems above. They however entail their own drawbacks, primarily in the form of increased computational time.

Reinitialisation

The initial value of the evolution equation is a signed distance function, however the solution after each time step is not. This means that each time step the scalar field becomes less smooth and the gradient is no longer guaranteed to be one, meaning it could become unbounded and lead to divergent results.

This can be solved by solving the Eikonal equation between every time step which means that the surface is re-smoothed each step. Analytically the reinitialisation does not affect the zero-level set so this procedure should not change the results of the interface evolution.

A reinitialisation process was presented by Sussman [81] in 1994, where instead of solving the Eikonal equation itself the new distance function is constructed by solving Eq. (37) to steady state.

$$\begin{aligned} \Phi_t &= S(\Phi^{(n+1/2)})(1 - |\nabla\Phi|) \\ \Phi(\bar{x},0) &= \Phi^{(n+1/2)}(\bar{x}) \end{aligned} \tag{37}$$

The solution of this provides the surface, Φ, for the next time-step. In the expressions above S is a continuous SDF and $\Phi^{(n+1/2)}$ is the scalar field (level set) resulting from one time-step of the evolution equation.

Velocity extension method

An important aspect of premixed combustion is that only the flame front has a propagation speed, while the flow has a continuous external velocity that is often irregular. The irregularity of the flow velocity can result in surfaces that become highly deformed. Since the G-equation has a propagation speed in addition to

the underlying flow velocity a method to maintain the smoothness of the surface involves extending the velocity at the front to the rest of the computational domain to guarantee that the gradient of the zero-level set is maintained.

For a level set function the velocity $\bar{v}$ is replaced by an extension velocity $\mathbf{u}_{ext}$ constructed using a coordinate along the normal direction to the interface and the velocity at the zero-level set.

In Ref. [75] a velocity extension method is presented based on the Fast Marching Method. The basic idea is to solve the equation

$$\nabla \Phi^{temp} \cdot \nabla F_{ext} = 0$$

so that Φ^{temp} is the SDF with the same zero level set as the original level set function Φ^n. This has a similar result to the reinitialisation method in practice, however, the key difference is that this method changes the velocity, not the scalar field Φ. Practically the equation above is solved in a similar way to finding the distance from grid points to the interface. The velocity is constructed as a weighted average of the speed values at the points which are used in computing the distance, where the weight is proportional to one over the square of the distance.

Adding source terms to the evolution equation

Another approach to maintaining the signed distance function is to change the evolution equation itself to build in the constraint $|\nabla \Phi| = 1$. This turns the Hamilton-Jacobi equation into a partial differential equation. Adding a source term that includes the solution function Φ itself does not affect the solution. This is because the only part of the level set function that is a solution to the front evolution equation is the zero level set, where Φ is identical to zero by definition, meaning the evolution equation is unchanged at the front.

This idea has been presented by Gomes and Faugeras in [23] for applications in surface reconstruction and image segmentation. It is also derived specifically for the G-equation in [67] where the added term to the evolution equation is referred to as a source term. This source function is determined using the above constraint.

The altered G-equation then looks as follows

$$\frac{\partial G}{\partial t} + \bar{u} \cdot \nabla G = S_L |\nabla G| + A(\bar{x},t) G \tag{38}$$

with

$$A(\bar{x},t) - \phi \nabla_i \phi \nabla_i A = \nabla_i \phi \nabla_i u_k \nabla_k \phi \tag{39}$$

Furthermore, the source term can be simplified as $\phi \to 0$ to

$$A(\bar{x},t) = \nabla_i \phi \nabla_i u_k \nabla_k \phi \tag{40}$$

Eq. (39) is the exact expression for A and therefore does not require reinitialisation. Sabelnikov et. al. show in [67] that this formulation is in fact equivalent to the velocity extension method. The advantage of this formulation is in the possibility to use the simplified version of the source term. In this form, however, the source term does not suffice to avoid reinitialisation, but it does require it less often which increases efficiency.

The G-equation is very frequently used when modelling turbulent flames in both the flamelet and the thin reaction zone regime, therefore it has attracted a lot of interest to improve upon the existing models and make them more robust and efficient. Different research groups have attempted to study the mathematical characteristics of the G-equation with the goal of increasing understanding of the physical connotations in combustion. The following are a few examples of the direction such research has taken.

Symmetries of the G-equation
Finding the symmetries of an equation is a way to describe the fundamental properties of the equation. A symmetry is a transformation under which the solution set of the equation remains invariant. One can find symmetries of different orders depending on the order of the transformations studied.

Finding symmetries of a particular differential equation is equivalent to finding transformations which map the equation onto itself. That is, finding a transformation that can be used to find new solutions of a given equation from known solutions.

Studying the symmetries of the equation can prove interesting when changes are made to the equation (source terms, averaging, etc). If the fundamental properties are changed one can argue that the new equation is no longer solving the same problem. They provide a way to make sure that the equation has not been fundamentally altered.

Oberlack et al. determines in [56] the different symmetries of the G-equation and then shows that the equation can be uniquely derived from these symmetries. The key symmetry in the derivation is

$$G^* = \mathscr{F}(G) \tag{41}$$

with

$$\frac{d\mathscr{F}(G)}{dG} > 0$$

This is denoted as the **generalised scaling symmetry**. This symmetry captures the fact that the value assigned to G at a given flame front is irrelevant as it lacks a physical meaning.

In [56] only point symmetries are addressed. In a later paper higher order symmetries are studied with the aim of finding conservation laws of the G-equation. It is concluded that there are no local conservation laws when the underlying flow velocity is allowed to be anything. However, when the velocity is constant an infinite number of conservation laws can be derived. The practical interest of these is in the potential to develop new numerical methods to solve combustion problems. [55]

Averaging the G-equation
Averaging is common practice when dealing with turbulent flows, so it is natural to want to get an average G-equation to deal with turbulent combustion. Problems arise however, because the G-equation lacks physical meaning outside the interface, the interpretation of the result of averaging is unclear. In addition, if interface averaging is done using the entire domain the results can be quite arbitrary [59] [44] [69] [32].

LES and the G-equation

Large Eddy Simulation (LES) is a simulation approach that only looks at the large scales of turbulence by filtering the smaller scales. This can be a problem for combustion as the flame front is generally much thinner than these scales. The zero level set of the G-equation is also much smaller than the LES filter size as it is just a sharp boundary, therefore some special care must be taken when using it.

That the G-equation is only valid at the zero-level set means that when averaging or filtering the flame front information should only be taken from the flame front itself, and not the rest of the G field. In the context of LES this means that a special filtering kernel that only takes information from the instantaneous flame surface should be used. In [61] a level set formulation is presented. By considering the symmetries of the G-equation described in [56] the formulation is shown to be consistent with the non-filtered G-equation.

The level set formulation presented by Pitsch [61] includes a number of unclosed terms that have to be modelled. These are the flame front conditionally averaged flow velocity, the subfilter burning velocity and the subfilter flame front wrinkling [61]. In [49] the LES formulation presented earlier is extended to account for turbulent transport. It is claimed that without this extension the G-equation is not able to capture the effects of turbulent transport.

Homogenisation of the G-equation

The propagation speed of the flame is an input to the G-equation model. This can be a problem when studying turbulent combustion, as the propagations speed is not necessarily known beforehand. In section 2.1.3 an expression for the displacement speed is derived combining the G-equation with a progress variable transport equation. However, the turbulent flame speed is still a much discussed topic in turbulent combustion. There are different definitions for it and it is not always clear how it is determined. The main point of interest is to quantify how the turbulence in the flow affects the burning velocity and front propagation.

Homogenisation is an attempt to analytically study the dependence of the front speed on the advection field, that is the underlying flow velocity. In [46, 12, 54, 86] the advection flow is assumed to be time-independent, enabling the study of the effect of turbulence on flame speed after a long time, i.e. the asymptotic growth rate $s_T = \lim_{t\to+\infty} G(x,t)/t$.

Homogenisation is about finding an explicit analytical expression for the limiting differential equation of a family of differential operators. Applying a scaling transform to the G-equation yields Eq (42).

$$G_t^\epsilon + \bar{v}(x/\epsilon) \cdot D_x G^\epsilon = s_l |D_x G^\epsilon| \tag{42}$$

The limiting differential equation is found by letting $\epsilon \to 0$. Homogenising the equation therefore gives us a value for s_T as defined above.

It has been proved that a limit for the G-equation can be found under certain assumptions for the underlying flow. This limit tends towards a scalar, which can then be considered to be the theoretical turbulent burning velocity. By changing the underlying flow, one can study how the burning velocity is affected. The main problem with this approach is the need for an analytic description of the underlying flow, and the assumptions of time-independence, divergence-free

flows and periodicity in space. This makes it difficult to apply in practical cases.

2.3.2 Flamelet model based on the G-equation and Z-equation

Li *et al.* [40] presented a flamelet model based on the G-equation and Z-equation. The model was used to simulate a partially premixed flame in a conical burner. Comparison with the planar laser-induced fluorescence (PLIF) experiments for the same burner indicated that the model can capture the flame structure and flame position reasonably well. The premixed part of the conical burner flame is small compared to the diffusion flame, it acts as an ignition point for the diffusion flame and provides stabilisation. The results were used to explain the performance of the conical burner [40, 4, 88]. The model can be summarised as follows:

- The solution of G-equation gives the $G = 0$ iso-surface (the position of the leading premixed flame front) at each time-step and its signed distance function. The solution of the Z-equation determines the position of the trailing diffusion flame. The intersection point of $G = 0$ and $Z = Z_{st}$ is defined as the triple-point of the partially premixed flame. Here, Z_{st} is the stoichiometric mixture fraction.

- The temperature and the composition in the region where $G < 0$ is given by the state of the unburned mixture.

- The burned region, where $G > 0$, is determined through a flamelet library tabulation method. As the premixed flame in this case is very small the flamelet library tabulation is essentially simplified to the flamelet library of a diffusion flame with the original fuel from one side and original oxidiser from the other side. On the other hand, when the leading premixed flame is large, the diffusion flame burns an intermediate fuel such as CO and H_2 on the fuel side and a mixture of oxidiser and products (CO_2, H_2O) on the oxidizer side.

2.3.3 Flamelet model based on the θ-equation and Z-equation

Bray *et al.* [99, 9] developed a model for turbulent partially premixed flames combining the progress variable equation with the mixture fraction equation. The basic assumption of the model is that the species composition and temperature can be determined by the two independent variables: θ and S. This can then be used to fully describe the flame structures. Based on this assumption a transport equation for the progress variable is derived from the original species mass fraction transport equations.

Combining these models gives rise to extra terms, such as the scalar dissipation rate χ and cross-scalar dissipation rate, in the equation. The cross-scalar dissipation rate is proportional to the scalar product of the gradient of mixture fraction and the gradient of the reaction progress variable. These terms have to be approximated through other models. Once the equations are set up, their solution can be used to determine the species distribution and the temperature field.

Application of this model to practical turbulent partially premixed flames has been rather limited.

2.4 Research questions

The overall aim of this thesis is to increase the understanding of turbulent partially premixed flames and to provide insights into modelling such flames. This is done by addressing some specific challenging issues.

- Detailed experimental and numerical studies on turbulent partially premixed flames are rather limited, in particular under high intensity turbulence conditions.

  Due to the limits in spatial resolution of velocity measurements, e.g. particle image velocimetry (PIV), eddies in the preheat and reaction zones are seldom detected. Recent experimental studies using multiple species planar laser-induced fluorescence (PLIF), e.g. the work at Lund University [42, 77, 100, 101], have shown a broadening of the reaction zones caused by turbulence at high Karlovitz number ($Ka > 100$). However, even so, the studies still lack simultaneous imaging of turbulent eddies in the reaction zones.

  The boundaries of the combustion regimes outlined in the previous section, based on dimensional analysis and scale comparison, have not been proven to be accurate. This is especially true for the thin reaction zone regime and the distributed reaction zone regime. Generally more studies are needed to determine where the boundaries of these regimes are, and whether the regimes are an accurate division.

- The present CFD models for turbulent partially premixed flames require more validation. The models discussed in sections 2.3.2 and 2.3.3 are based on the assumption that the structures of turbulent partially premixed flames can be described using two independent variables, G and Z or θ and Z. This assumption needs to be proven. Bray *et al.* [99, 9] suggested the use of reaction progress variables other than the normalized temperature. This illustrates that the reaction progress variable is not uniquely defined when discussing turbulent partially premixed flames, leading to question of whether different progress variables perform differently in CFD models.

- As mentioned before, in G-equation based models, the local displacement speed is an input required by the model. Since current experiments cannot directly measure the local displacement speed of a turbulent flame due to the two-dimensional nature of most laser based experiments, a systematic study of the local displacement speed in turbulent partially premixed flames is necessary, especially at high Karlovitz number conditions, as these are the flames most common in engineering applications.

- As a clean fuel possibly obtainable from renewable sources, hydrogen has the potential to become an important fuel for combustion engines in the future. Hydrogen combustion is a complex process. Due to hydrogen's high diffusivity thermal-diffusive instabilities are common [76], making hydrogen combustion more difficult to control. In order to counteract such effects the structure and propagation of turbulent hydrogen partially premixed flames requires further investigation.

In this thesis we carried out direct numerical simulations (DNS) of two flames, a methane/air turbulent partially premixed flame and a hydrogen/air

turbulent partially premixed flame, both at high Karlovitz number conditions. The DNS data provides detailed information about the structures and propagation of the flames that can be used to answer the questions listed above.

3 DNS of turbulent partially premixed flames

This section will present a general overview of direct numerical simulations (DNS) as well as a detailed description of the cases studied in this thesis.

The basic idea of DNS is to use a high accuracy numerical method to solve the governing equations of turbulence and, when studying reacting flows, the chemical reactions. The name alludes to the fact that DNS resolves even the smallest scales of turbulence, meaning that there is no need for sub-grid scale turbulence modelling. In addition, combustion also has the requirement to resolve the smallest flame scales, that means that if the flame thickness is less than the Kolmogorov scale it will set the resolution requirements for DNS.

The smallest scales found in turbulent partially premixed flames can be any of the following three, depending on the Karlovitz number: the Kolmogorov length scale, the leading front premixed flame thickness (for the preheat zone and the reaction zone) and the thickness of the mixing layer/reaction zone in the trailing diffusion flame. Through observation, the latter is expected to be larger than the former two regardless of Ka and therefore will not be discussed further. In the flamelet regime, where $Ka < 1$, the smalles scale is the premixed flame thickness. The flame in this regime is a sharp boundary and the smallest turbulent eddies are too large to disturb the internal flame structure. When Ka is high the Kolmogorov scale is smaller than the flame thickness and therefore the flame is also completely resolved by the DNS. In such a case the spatial resolution necessary for the Kolmogorov scale is of the same order of magnitude as $Re_0^{9/4}$.

Due to the resolution required, DNS is very computationally expensive and supercomputers are needed to perform the simulations. The DNS runs presented in this thesis were carried out on the Prace Tier-0 computers CURIE TN, based in France at the TGCC (Très Grand Centre de calcul du CEA). Each run required about 3 million CPU hours.

3.1 Governing equations

Turbulent reacting flows are governed by the conservation equations of mass, momentum, species and energy as well as an equation of state. The numerical approach used for these simulations splits pressure into two parts: a thermodynamic pressure, $P(t)$ and a hydrodynamic pressure, $p_h(\mathbf{x},t)$. The thermodynamic pressure is constant and used in the equation of state. The smaller hydrodynamic pressure is used in the momentum equation. The continuity equation can be written in material derivative form as this makes it possible to handle large density gradients.

$$\frac{1}{\rho}\left(\frac{\partial \rho}{\partial t} + u_i \frac{\partial \rho}{\partial x_i}\right) = -\frac{\partial u_i}{\partial x_i}$$

$$\rho\left(\frac{\partial u_i}{\partial t} + u_j \frac{\partial u_i}{\partial x_j}\right) = -\frac{\partial p}{\partial x_i} + \frac{\partial}{\partial x_j}\left(\mu\left(\frac{\partial u_i}{\partial x_j} + \frac{\partial u_j}{\partial x_i} - \frac{2}{3}\frac{\partial u_k}{\partial x_k}\delta_{ij}\right)\right)$$

$$\rho\left(\frac{\partial Y_k}{\partial t} + u_j \frac{\partial Y_k}{\partial x_j}\right) = -\frac{\partial \rho Y_k V_{kj}}{\partial x_j} + \dot{\omega}_k \tag{43}$$

$$\rho C_p \left(\frac{\partial T}{\partial t} + u_j \frac{\partial T}{\partial x_j} \right) = - \sum_{k=1}^{N} h_k \dot{\omega}_k - \left(\rho \sum_{k=1}^{N} C_{p,k} Y_k V_{kj} \right) \frac{\partial T}{\partial x_j} + \frac{\partial}{\partial x_j} \left(\lambda \frac{\partial T}{\partial x_j} \right)$$

$$P = \rho \Re T \sum_{k=1}^{N} \frac{Y_k}{W_k}$$

where the spatial coordinate is denoted by x and time t. ρ, μ, C_p and λ are the mixture averaged density, dynamic viscosity, heat capacity and conductivity of the mixture, respectively. u_i is the velocity component i and δ_{ij} is the Kronecker delta. Y_k, $\dot{\omega}_k$, h_k, $C_{p,k}$ and W_k are, in order, mass fraction, reaction rate, specific enthalpy, heat capacity and molar mass of species k. T is temperature, N is total number of species and $\Re$ is the universal gas constant. Species diffusion is given by

$$-Y_k V_{kj} = D_k \frac{\partial Y_k}{\partial x_j} - Y_k \sum_{i=1}^{N} D_i \frac{\partial Y_i}{\partial x_j} \tag{44}$$

where D_k is the mixture averaged diffusion coefficient of species k.

3.2 Chemistry and transport properties

When carrying out simulations of reacting flows a choice can be made when it comes to the chemical mechanism used to describe the reactions. The simplest approach is to use one step chemistry, this means that the reactants are directly turned into products by the reaction. Single step chemistry is computationally inexpensive and in many cases contains sufficient information for practical applications. However, because it does not include any intermediate species it cannot be used when studying partially premixed flames.

In the other extreme there are complete chemical reaction mechanisms. These include all possible paths for the reactants to reach the state as products. Chemical reaction mechanisms are generally very extensive, e.g. the methane-air reaction mechanism from GRI-Mech 3.0 consists of 325 reactions that involve 53 species.

Detailed chemistry is necessary when studying methane partially premixed flames because the diffusion flame burns an intermediate fuel, not the original fuel. However, complete mechanisms are computationally unwieldy due to the number of species and reactions present. In order to be able to study the effects of chemistry on a turbulent flame so-called skeletal mechanisms have been developed, these aim to maintain the species that have the greatest impact on behaviour of the flame and remove everything else, thereby achieving a middle ground between accuracy and computational viability.

In this study, the CH4/air mechanism by Smooke and Giovangigli [78], employing 16 species and 25 reactions (10 reversible and 15 irreversible reactions), is used for the methane flame. For the hydrogen flame the H2/air mechanism by Li *et al.* [41], employing 9 species and 21 reversible reactions, is used.

The transport properties, e.g., species diffusion coefficients, thermal conductivity, and viscosity, are mixture averaged based on the individual species obtained from the Chemkin thermodynamic database [31].

3.3 Numerical Methods

The numerical methods used to solve the governing equations in this study consist of a low Mach number DNS solver [94] with a stiff solver for the chemical reaction calculations.

The temporal integration of the convection-diffusion-reaction system is based on a 2nd order symmetrical Strang splitting algorithm. For each time-step, Δt the stiff chemical reaction term is calculated. Between these steps intermediate integrations of the diffusion and convection terms are carried out with a time-step $t_{1/2} = \Delta t/2$. The integration of the diffusion term is split further into multiple sub-steps of explicit integrations, starting with a Runge-Kutta step followed by Adams-Bashforth steps. This sub-step size is chosen to satisfy the diffusion stability limit.

All spatial discretization is based on a 6th order central difference scheme, except for the discretization of the convective terms in the species, mass and energy equations where a 5th order weighted essentially non-oscillatory (WENO) scheme is used to avoid non-physical numerical oscillations. Any necessary interpolation is done with a 6th order scheme. The pressure/velocity decoupling results in a variable coefficient Poisson equation that is solved using an efficient parallel multigrid method [92]. The temporal/spatial accuracy of the solver has been verified using successive grid/time-step dependency tests. The solver has been used in several earlier studies of both laminar and turbulent flames [91, 90, 98, 16, 15].

The integration of the stiff system of equations for the chemical reaction rates is done using the DVODE solver [10].

3.4 Case Description

Two 3D DNS runs have been carried out, one for a methane/air turbulent partially premixed flame and one for a hydrogen/air turbulent partially premixed flame. The ambient pressure is 1 bar for both flames, and the unburned gas temperature is set to $T_u = 298\ K$.

In order to obtain a steady state initial condition for the 3D DNS a laminar 2D DNS simulation of the same mixture was run first. The 2D-DNS study was performed in a rectangular domain with a stream-wise (x-direction) length (L_x) of 20 mm and a cross-flow (y-direction) width (L_y) of 10 mm. A convective outflow condition was used at the outlet and at the cross-flow boundaries periodic boundary conditions were imposed. The uniform inflow velocity was varied during the transient stage of the simulation until a stabilized flame with leading edge at $x = L_x/4$ was obtained. The equivalence ratio at the inflow boundary, Φ_{in}, was stratified following the Gaussian function of y given in Eq. (45), where $c = 0.17$.

$$\Phi_{in} = C_f \cdot exp(-((y - L_y/2)/L_y)^2/(2c^2)). \tag{45}$$

where C_f is a constant that controls the maximum equivalence ratio in the domain. For the methane/air flame $C_f = 1.5$ and for the hydrogen/air flame $C_f = 3$. This definition results in a stratified equivalence ratio profile with $\Phi_{in} = 1.5$ for the methane/air flame and $\Phi_{in} = 3$ for the hydrogen/air flame at the centreline and zero at the cross-flow boundaries.

	methane/air flame	hydrogen/air flame
L_x [mm]	20	20
L_y [mm]	10	10
L_z [mm]	10	10
C_f	1.5	3
n_f	12	12
T_u [K]	298	298
V_u [m/s]	4.5	3
ℓ_0 [mm]	1.667	1.667
u'_0 [m/s]	8.5	10
τ [ms]	0.196	0.1667
Re_0	83	21
$Ka_{\Phi=1}$	55	5.5
$Ka_{\Phi_{max}}$	665	4.7

Table 1: Summary of simulation set-up and initial conditions.

In the 3D-DNS, a lateral (z-direction) dimension was added ($L_Z = 10$mm) and $\Psi = [\mathbf{u}\ T\ \mathbf{Y}]$, where $\mathbf{u}$ is velocity, T is temperature, and $\mathbf{Y}$ is species mass fractions, from the 2D-DNS steady solution were imposed as initial conditions as it was extended homogeneously in the lateral direction: $\psi_{3D}(x,y,z) = \psi_{2D}(x,y)$.

The velocity field is made up of two parts, a mean velocity field and a fluctuating velocity. At the inlet plane the mean flow velocity was set to V_u. The fluctuating velocity was obtained from synthesizing Fourier waves [38, 93] satisfying a prescribed turbulence energy spectrum [27] in a cubic box with periodic boundary conditions. The same synthesized turbulence was used to initialize the fluctuating flow field.

When initialising the turbulence field the integral length scale, ℓ_0, was set to $\ell_0 = L_x/n_f$ where n_f is the number of integral eddies found in the stream-wise direction of the computational domain. The turbulent integral scale velocity, u'_0, was specified. The integral time scale $\tau \sim \ell_0/u'_0$.

Table 1 summarises the specific parameters of the two DNS cases, including the Reynolds number based on the integral scale and the Karlovitz number defined at the triple flame front $\Phi = 1$ and at the rich premixed flame near the centreline, around $\Phi = 1.5$ for methane and $\Phi = 3$ for hydrogen.

The 3D domain was discretized on a uniform grid of $1024 \times 512 \times 512$ (in the x, y and z directions) cubic cells. This yields a total of approximately 268 million cells with a grid resolution of $\Delta s = 19.4\mu m$. The computations are run for two integral times, $t \leq 2\tau$. Since no forcing is used, the turbulence field decays from its initial intensity during the first 1.5τ before stabilising. This results in a Karlovitz number that decreases with time, reaching its lowest values of 40 for $\Phi = 1$ and 500 for $\Phi = 1.5$ at $t/\tau = 2$, still well above the limit into the flamelet regime.

4 Results and Discussion

In order to describe the structures of partially premixed flames we first introduce the two reaction scalars that can be used to identify different parts of the flame. Mixture fraction or equivalence ratio is a suitable choice to track the trailing non-premixed flame. The equivalence ratio and mixture fraction for a hydrocarbon or a hydrogen flame can be determined from the local element mass fractions of H, C, O, and N. The equivalence ratio Φ at a given point in the flow field is given by

$$\Phi = \left(\frac{2Y_C}{W_C} + \frac{Y_H}{2W_H}\right) / \left(\frac{Y_O}{W_O}\right), \tag{46}$$

where Y_i and W_i are the mass fraction and the mass weight of element i, respectively. The mixture fraction Z is defined as,

$$Z = \frac{Y_C + Y_H}{Y_C + Y_H + Y_O + Y_N} = Y_C + Y_H. \tag{47}$$

The trailing non-premixed flame is located at $\Phi = 1$, which is equivalent to the mixture fraction $Z = Z_{st}$. Since the two scalars are equivalent when tracking the diffusion flame, either one can be chosen for the analysis. In this study equivalence ratio is chosen as it also provides information for the analysis of the premixed front.

The leading premixed flame front can be identified using the fuel mass fraction, since the fuel is oxidized in the reaction zone of the premixed flame. Due to the fuel being stratified in the unburned mixture, the progress of fuel consumption is a function of local equivalence ratio. A normalised fuel mass fraction that considers local equivalence ratio is introduced as a reaction progress variable.

$$c_1 = \frac{Y_{F,u} - Y_F}{Y_{F,u} - Y_{F,b}}, \tag{48}$$

where Y_F is the mass fraction of fuel, $Y_{F,u}$ and $Y_{F,b}$ are the mass fractions of fuel at the corresponding unburned state and the completely burned state, respectively.

$$Y_{F,u} = \frac{\Phi W_F}{\Sigma W_{i,r}} \quad \text{and} \quad Y_{F,b} = \begin{cases} \frac{(\Phi-1)W_F}{\Sigma W_{i,p}} & \Phi > 1 \\ 0 & \Phi \leq 1 \end{cases} \tag{49}$$

where $W_{i,r}$ and $W_{i,p}$ are the molecular weight of the reactant species and the product species, respectively.

Note that $Y_{F,b}$ is a reference mass fraction of the fuel remaining in the burned gas determined using a one-step irreversible reaction model. As mentioned in the previous section, in real hydrocarbon fuel chemistry the fuel is first converted to intermediate species. The presence of intermediates such as CO and H_2 means that Y_f can be zero even when $\Phi > 1$. In this way $Y_{F,b}$ takes into account combustion intermediate species even if it is based on the one-step irreversible reaction model.

The local displacement speed of the iso-surface $Y_F = Y_{F,f}$, where $Y_{F,f}$ is a constant chosen for the analysis, can be determined using the level-set method discussed in section 2.3.1.

The displacement speed is defined as

$$S_D = -(\rho_u^{-1} \mid \bigtriangledown Y_F \mid^{-1} \rho \frac{D}{Dt} Y_F) \mid_{Y_{F,f}} = S_{D,diff} + S_{D,react},$$

$$S_{D,diff} = -(\rho_u^{-1} \mid \bigtriangledown Y_F \mid^{-1} \bigtriangledown \cdot J_F) \mid_{Y_{F,f}} \tag{50}$$

$$S_{D,react} = -(\rho_u^{-1} \mid \bigtriangledown Y_F \mid^{-1} \dot{\omega}_F) \mid_{Y_{F,f}}$$

The negative sign is added since the mass fraction of fuel decreases as a function of the reaction progress variable, it thereby ensures that S_D is positive when propagating towards the unburned mixture. D/Dt is the material derivative and J_F and $\dot{\omega}_F$ are the diffusive flux of the fuel and the net reaction rate of fuel, respectively. S_D consists of a reaction part ($S_{D,react}$) and a diffusion part ($S_{D,diff}$) and is affected by curvature, strain, equivalence ratio, etc. It is therefore important to scrutinise which quantities have the largest effect on the displacement speed of partially premixed flames and whether they differ from their premixed counterparts.

It should be noted that the iso-surface of the fuel mass fraction does not coincide with the iso-surface of the reaction progress variable c_1, due to the normalisation. The displacement speed of the iso-surface of the reaction progress variable c_1 can be used to characterize the flame propagation more accurately,

$$S_D = (\rho_u^{-1} \mid \bigtriangledown c_1 \mid^{-1} \rho \frac{Dc_1}{Dt}) \mid_{c_f}, \tag{51}$$

where c_f is a reference constant for the iso-surface used in the analysis. When local displacement speed is analysed, the choice of iso-surface is crucial and therefore it is important to clarify what iso-surfaces have been considered in this study.

Previous studies have reported that the propagation of the premixed flame is affected strongly by the local curvature of the flame. The curvature of the flame surface can be defined using the iso-contour of the progress variable,

$$\kappa = \nabla \cdot n, n = \nabla c_1 / |\nabla c_1|. \tag{52}$$

4.1 Methane/air partially premixed flame

Results from direct numerical simulations of three-dimensional flames with a skeletal chemical mechanism provide a detailed picture of the structure and dynamics of a partially premixed methane/air flame in turbulence. The results are analysed with respect to the following aspects: (a) triple flame structure and interaction between the diffusion flame the premixed flame; (b) detailed reaction layers and the impact of elementary reactions; (c) the displacement speed and its correlation with local equivalence ratio and curvature; (d) modelling of the flames.

4.1.1 Structures of the flame

Figure 5 shows a snap-shot of the three dimensional leading premixed flame front at $t/\tau = 1$. The flame front is visualized using the iso-surface of $c_1 = 0.95$, where c_1 is the progress variable defined in Eq. (48). The temperature at the flame is shown using the colour distribution on the surface. The 2D plane behind

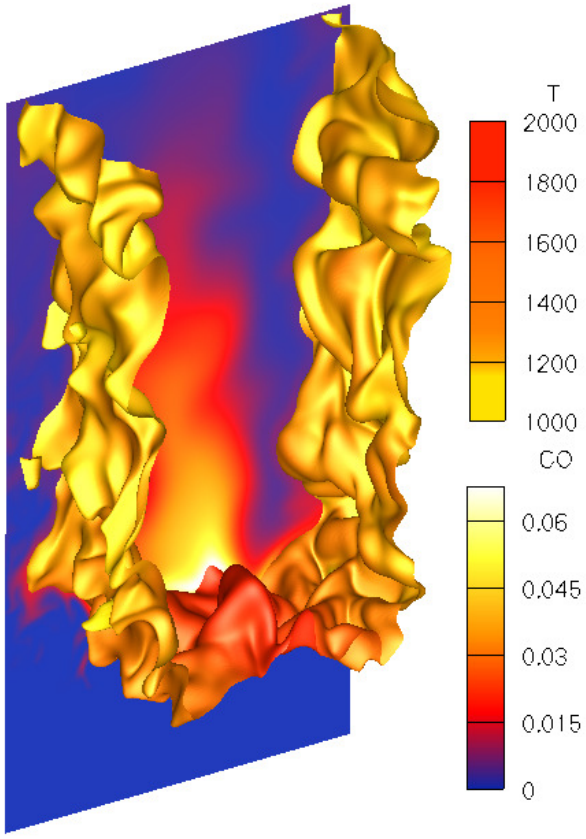

Figure 5: Premixed flame surface coloured with temperature and distribution of CO mass fraction in the central plane. Results are taken at $t/\tau = 1$.

the flame surface shows the mass fraction of CO to indicate the position of the diffusion flame. The flow direction is from the bottom of the figure to the top, and the flame is propagating downwards. The leading front has a W-shaped structure, indicating that the flame propagates with a lower displacement speed along the centreline and the edge than in between these points.

The equivalence ratio on the flame surface varies between 0.38 and 1.25, using the definition of equivalence ratio in Eq. (46). The fuel-rich part ($\Phi > 1$) is in the center of the domain and the lean part ($\Phi < 1$) at the edge of the flame. The flame is wrinkled as a result of turbulence/flame interaction. The wrinkles occur at fairly large scales. At the trailing edge two lean premixed flames are found to burn at $\Phi \simeq 0.39$. This is significantly lower than the lean flammability limit for methane/air flames ($\Phi \sim 0.53$) reported in literature [22]. These trailing lean premixed flames persist until the end of the domain.

To examine the structure of the diffusion flame and the interaction between the diffusion flame and the premixed flame Figs. 6 and 7 show the mass fraction of CH_4, O_2, H_2, CO and OH radicals as well as temperature in relation to the iso-line of $c_1 = 0.95$. The distributions are shown for the same 2D plane and at same instance of time as in Fig. 5. The diffusion flame is demonstrated by the CO, H_2, O_2, and OH distribution.

Previous studies of laminar partially premixed flames [5] and turbulent fuel-rich premixed flames [53] indicate that CO and H_2 are combustion intermediates found downstream of rich premixed flames. From Figs. 6 and 7 it is clear that CH_4 is consumed completely at the premixed flame front.

CO and H_2 are formed in the rich part of the premixed flame where there is a deficit of oxygen. The flame is thus unable to complete the oxidation of the intermediate fuels. The oxidation of CO and H_2 requires oxygen from the lean part of the flame. The oxygen surplus from the trailing lean premixed flame reacts with H_2 downstream of the rich part of the flame providing the radical pool that completes the oxidation of combustion intermediates such as CO and H_2. Figs. 6 and 7 show that the diffusion flame is located around $\Phi = 1$, where CO and H_2 are oxidized and OH has its local maximum mass fraction.

Kioni *et al.* [33] and Owston and Abraham [57] studied the species distributions in a triple-flame and compared it with premixed flames with different equivalence ratios. It was suggested that the diffusion flame reaction zone could aid in extending the flammability limits by providing non-flammable regions with radicals, thereby increasing reaction rates [57]. The OH distribution in Fig. 6 makes it clear that the diffusion flame supports the lean trailing premixed flame. The OH radicals peak at the diffusion flame, suggesting they are formed there. These radicals are diffused in the burned gases until they reach the lean premixed trail. The neighbouring lean premixed flame (result of the periodic boundary conditions) does not provide support to the flame in the form of OH radicals, thus it has no obvious role in maintaining the trailing premixed flame.

The temperature is the highest in the tip of the diffusion flame where oxidation of CO and H_2 is more complete. On the surface of the premixed flame (Fig. 5) the temperature varies from its highest values ($\simeq 2000$ K) at the base of the flame to progressively lower ($\simeq 1200$ K) along the lean trail. The temperature at the lean trail is low; however, the flame is stable as it is sustained by its neighbouring diffusion flame as discussed earlier.

Fig. 6 shows that high concentrations of CO and H_2 can be found on the

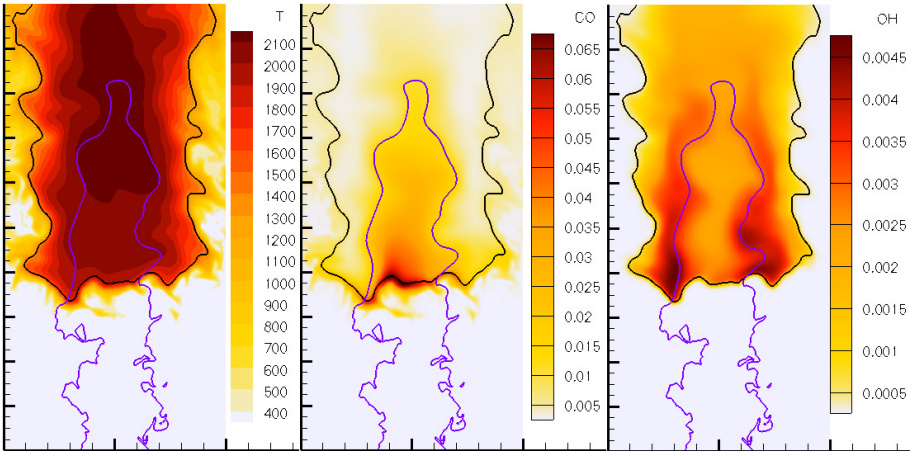

Figure 6: Distribution of temperature, mass fractions of CO and OH radicals in the central plane. The solid black line is the iso-line of $c_1 = 0.95$ in the plane; the solid purple line is the iso-line of $\Phi = 1$ in the plane. Results are taken at $t/\tau = 1$.

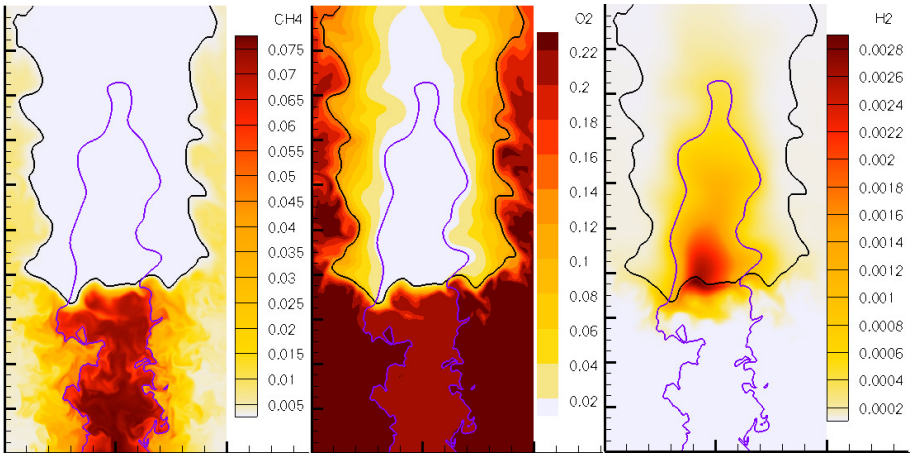

Figure 7: Distribution of mass fractions of CH_4, O_2 and H_2 in the central plane. TThe solid black line is the iso-line of $c_1 = 0.95$ in the plane; the solid purple line is the iso-line of $\Phi = 1$ in the plane.. Results are taken at $t/\tau = 1$.

unburned side of the lean premixed flame, where $c_1 < 0.95$. These regions correspond to areas of high temperature. Despite the high temperature there are no reactions occurring, which can be seen as there are no OH radicals present in these zones. This means that these areas are the preheat zone of the leading premixed flame. That these zones exist as small islands relatively far from the flame indicates that the preheat zone is broadened by turbulent eddies.

The islands of the high CO and H_2 concentration, and high temperature, act as a trace marker for the eddies originally formed in the reaction zone that are transported to the preheat zone. The Karlovitz number for this flame ranges from 55 to 665, therefore, according to the theory discussed in section 2.2.2 it is possible for the small eddies to exist in the preheat and reaction zones. These results support the boundaries of the regime diagram of turbulent premixed flames developed based on dimensional analysis.

In previous studies of partially premixed flames it has been noted that using a progress variable based on fuel does not necessarily capture the diffusion flame, and conditioning on various species distributions does not provide a viable alternative as no single species can clearly show the triple flame structure [64]. In the present flame it is clear from Figs. 5 and 6 that the fuel based progress variable cannot ascertain the position of the diffusion flame, since the fuel in the rich part of the premixed flame has been converted to intermediate species. To account for this a new progress variable based on the final combustion products is suggested,

$$c_2 = (Y_{CO_2} + Y_{H_2O})/\alpha, \quad \alpha = \begin{cases} 5 \cdot \frac{\Phi}{\Phi+\gamma}, \Phi < 1 \\ \frac{5}{\Phi+\gamma}, \Phi \geq 1 \end{cases} \tag{53}$$

where γ is the mass ratio of air to fuel at stoichiometry.

Figure 8 shows the time evolution of the flame and its reaction zone structure (visualised with production/consumption rate of H radicals, $\dot{\omega}_H$). The diffusion flame and the lean trailing flames are clearly visible in the $\dot{\omega}_H$ field. The iso-contours of c_2 are also plotted in Fig. 8. It appears that c_2 can be used to identify the diffusion flame front as well as the premixed one. The progress variable iso-lines reflect the fact that chemical reactions take place over a large region behind the main premixed flame front as the progress variable does not reach one until these reactions are completed. Note, however, that the reaction rates of H in the downstream reaction zones shown in the figure are two orders of magnitude weaker than those at the leading premixed flame front.

Several authors [34, 87, 29, 28, 84] have studied the effect of strain on the structure of a triple flame and its propagation. It is observed that the diffusion flame is much weaker than the premixed front (heat release rate is about 2 orders of magnitude lower) [84]. This is explained by a low scalar dissipation rate [84]. This is consistent with the present flame as the reaction rate of H formation in the diffusion flame is indeed two orders of magnitude lower than that in the premixed flame.

At the initial time the flame is essentially laminar due to the initial conditions imposed; it consists of a main premixed flame front, $0.5 < \Phi < 1.25$, trailed by two thin lean premixed flames at the edges and a diffusion flame following the stoichiometry line. The net reaction rate of H radicals shows distinct reaction zone structures: (a) a thin H production layer at the premixed flame front and the trailing diffusion flame front (around $\Phi = 1$), (b) a thinner layer of

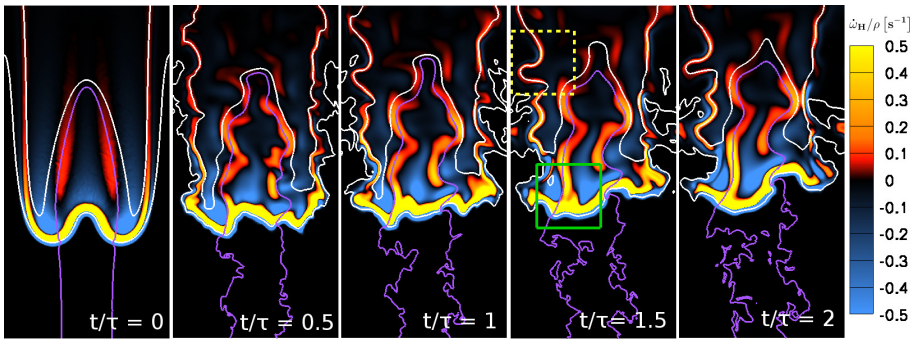

Figure 8: View of the centre plane at different times showing the location of the triple flame visualised with reaction rate of H. τ is the eddy turnover time. Iso-lines for $c_2 = 0.5$ and $c_2 = 0.93$ are drawn in white. Local equivalence ratio $\Phi = 1$ is shown with a purple line. Close-ups to the boxes are shown in Fig. 9.

H consumption upstream of the H production layer, and (c) a rather thick H consumption layer in between the premixed flame and the diffusion flame. The overall structure of the flame remains similar throughout the flame evolution in time.

In different parts of the flame the relative importance of different elementary reactions varies due to the difference in temperature and composition of the mixture. In the H-production layer of the leading premixed flame front the main reactions responsible for the net production of H are $H_2 + OH = H_2O + H$ and $CO + OH = CO_2 + H$, regardless of equivalence ratio. The main difference found along the premixed front is the strength of these reactions at the different parts of the flame, the highest net rates are found at the rich part of the flame. This is the CO-H_2 oxidation layer, which is characterized by the high net H production rate in Figure 8. H_2 and CO are formed in the thin H-consumption layer upstream of the CO-H_2 oxidation layer, where the net consumption of H is mainly a result of the $H + O_2 = O + OH$ reaction. In addition, in rich parts of the flame $CH_4 + H = CH_3 + H_2$ is significant, while $H + O_2 + M = HO_2 + M$ is important in the lean part and $CH_3 + H = CH_4$ dominates at the stoichiometric part of the flame.

The same reactions account for the production of H in the diffusion flame. The net rates of reaction are however much lower here than in the leading premixed front; the reversible reactions $H + O_2 = O + OH$, $H_2 + OH = H_2O + H$ and $O + H_2 = OH + H$ are close to equilibrium.

The lean trailing premixed flame is significantly different from the leading front of the flame, the main reactions responsible for the production of H in the lean trailing premixed flame are $CH_3 + O = CH_2O + H$ and $HCO + M = CO + H + M$. The strongest individual net reaction of the lean trail is $H + O_2 = O + OH$, an H-consuming reaction. The consumption region found behind the leading premixed flame are a result of $H + O_2 + M = HO_2 + M$ and $H + HO_2 = 2OH$ reactions.

The reaction rate of H radicals directly behind the premixed front up to the diffusion flame is negligible in the initial flame (when the flame is laminar). This is because the different elementary reactions producing and consuming H are in

equilibrium resulting in no net H reaction rate. However, in the turbulent flame this region of equilibrium is not maintained due to turbulence/flame interaction.

In Fig. 9 close-ups of the triple flame and the lean trail are presented to show the distribution of three key species and the heat release rate in the neighbourhood of the flame surface.

The maximum CH_2O mass fraction found in both parts of the flame is of similar magnitude, however, in the lean trail it is found to spread out to a larger region. The spread of high CH_2O mass fraction coincides with the high temperature of the fuel/air mixture. The CH_2O is found at temperatures up to $\simeq$1600 K. In the rich part of the main leading premixed flame front CH_2O can be found at higher temperatures than in the rest of the flame, while in the lean trail there is little left above 1200 K.

Downstream of the lean part of the premixed front the mass fraction of OH is high. This state coincides with the negative reaction rate of H in Figure 8. The temperature of the lean fuel mixture increases further downstream due to the two neighbouring flames; this combined with the radical support from the diffusion flame, providing OH and other reactive species, allows the lean trail to burn despite its low equivalence ratio.

H_2 is produced at the rich premixed flame and consumed at the diffusion flame; the diffusion of H_2 is fast and it can be found throughout the region between the lean trail and the diffusion flame. The mass fraction of H_2 at the lean trail is low, which indicates that H_2 is consumed in the lean trail. The lower frames in Fig. 9 show that the heat release rate for the lean flame is two orders of magnitude lower than that of the main premixed front. Note that the heat release rate for the premixed flame is much stronger than that of the diffusion flame trailing the triple point. The weaker heat release rate downstream of the premixed front is also more distributed, making it difficult to identify a distinct flame. A comparison with Fig. 8 implies that the parts along the lean trail where there is no production of H are not necessarily quenched; in fact, the heat release rate in one of these segments is higher than the surroundings, where there is H production. The heat release rate is strengthened in areas of high curvature convex to the burnt gases.

4.1.2 Local displacement speed: triple flame acceleration

An important property of partially premixed flames is the displacement speed of the flame (S_D). A triple-flame front is commonly observed in certain partially premixed flames, e.g. in lifted non-premixed jet flames where triple-flame propagation plays an important role in the flame stabilisation process and consequently the lift-off distance [59]. The triple flame structure is clearly identified in the present flame using the progress variable c_2 defined in the previous section. The propagation speed of the triple flame is expected to be different from that of a stoichiometric premixed flame of the same fuel. It depends on various parameters, including the Lewis number [11, 39] and mixture fraction gradient [25, 34]. Ko and Chung [35] have experimentally observed that the displacement speed of a methane/air triple flame is several times larger than the laminar flame speed. In this section we examine the displacement speed and its correlation with local equivalence ratio and flame curvature.

In Fig. 10 the contributions to displacement speed from the reaction and the diffusion parts are shown for a segment of the premixed flame front that in-

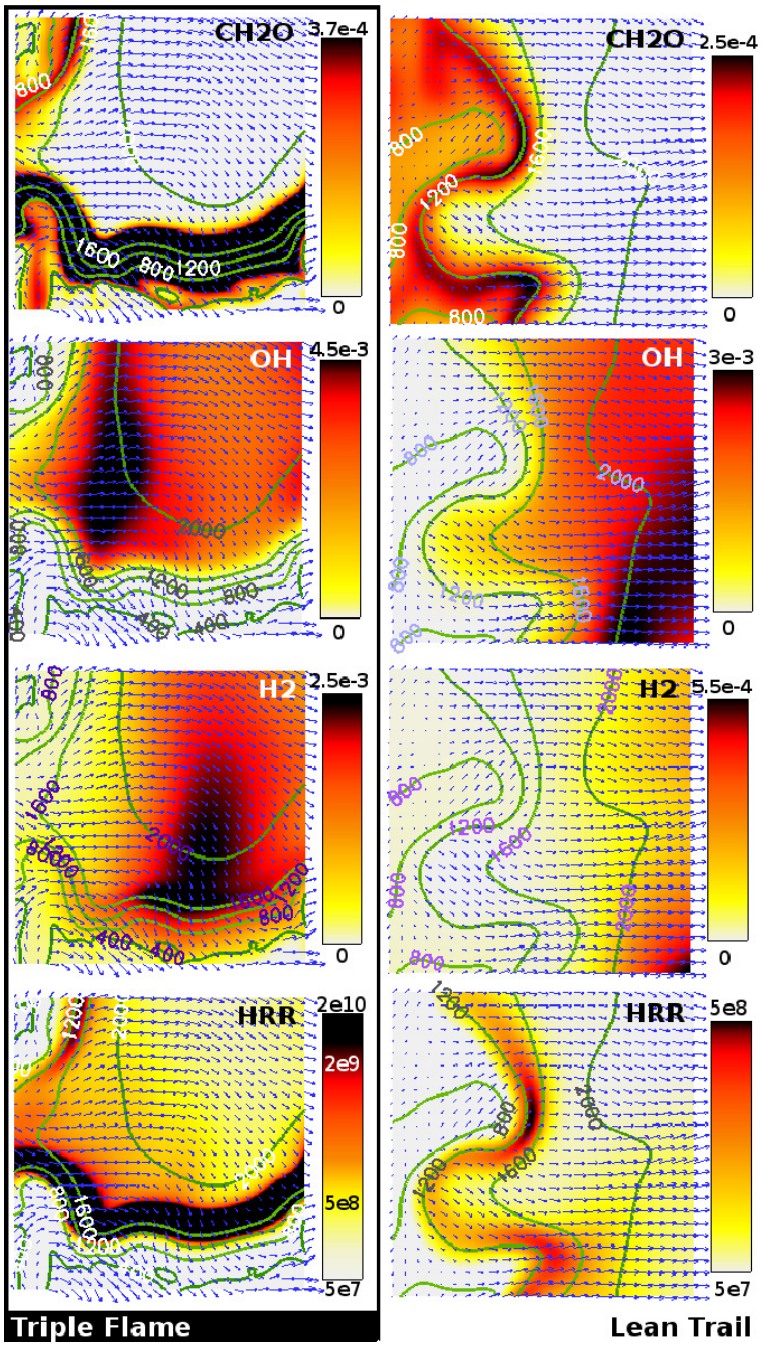

Figure 9: Close-up to the areas in Fig. 8 showing species distributions at the leading premixed flame front (left column) and in the lean trail (right column). Vectors show the instantaneous local velocity. Iso-lines showing temperature.

cludes the triple point. A large spatial variation is observed in both the reaction part of the displacement speed (middle, Fig. 10) and the diffusion part of the displacement speed (bottom, Fig. 10). The reaction part of S_D is correlated to both the equivalence ratio, with the strongest reactions happening close to stoichiometry, and the curvature of the flame front. Strengthening of $S_{D,react}$ can be seen in the parts of the flame curving towards the burnt gases. On the other hand, cusps are formed behind the parts that curve towards the unburned gases. The effects of both curvature and equivalence ratio will be further addressed in Figs. 11 and 12. The diffusion component of the displacement speed (bottom, Fig. 10) shows large spatial variation at smaller length scales, which appear to be related to turbulence. The effect of diffusion on the total displacement speed (top, Fig. 10) is significant in all regions of the flow field, especially in the unburned gases. The reaction rate contribution is strongest in the reaction zone. Displacement speed shows large variations not only along the flame but also across, in the flame normal direction. This makes the choice of iso-surface for the evaluation of S_D very important. Discussion regarding the choice of iso-surface can be found in connection to Figs. 13 and 14.

Fig. 11 shows that negative displacement speeds, i.e., when the iso-surface moves away from the unburned mixture, correspond to regions where the flame is convex towards the unburned gases. Such structures lose heat through diffusion to the cold unburned mixture leading to lower displacement speeds. Curvature is found to have a strong correlation to displacement speed for all Φ in this case. Negative displacement speed have been previously reported in [18].

Fig. 11 shows a scatter plot of displacement speed as a function of curvature conditioned on different Φ at $t/\tau = 1.5$. The straight lines show the correlation at initial time. A clear positive correlation of increasing displacement speed with curvature is seen (positive curvature is referred here to as convex to the burned gases). The relation is clearly monotonic and negative displacement speeds are consistently found at flame segments of negative curvature. This relation is also implied in Fig. 9, where high curvature parts of the flame have higher heat release rates. The reaction component of the displacement speed is always positive, therefore it is inferred that the negative displacement speeds are caused by the effect of curvature on the diffusion term in the formulation of displacement speed.

In Fig. 11 we can also see that the dependence of displacement speed on curvature is highly dependent on time. At the initial time the correlation is similar for all Φ conditions, however, they develop differently in time. Most noticeable is that the gradient of the correlation for the rich flame increases for positive curvature. The rich flame in this case coincides with a very high heat release rate. This is a result of the leading premixed flame front being connected to the diffusion flame, as can be seen in figures 8 and 9. The highest displacement speed is found to be several times higher than the corresponding unstretched laminar premixed flame. This result is consistent with previous experiments [7].

In Fig. 12 the displacement speed dependency on equivalence ratio is studied by conditioning on zero curvature. The laminar flame speed is calculated for a 1D planar unstretched flame using the same chemical mechanism as in the DNS. It is shown that the displacement speed from the partially premixed flame is generally lower than the laminar flame speed of the unstretched premixed flame, except in the lean regions where the corresponding 1D methane-air mixture at

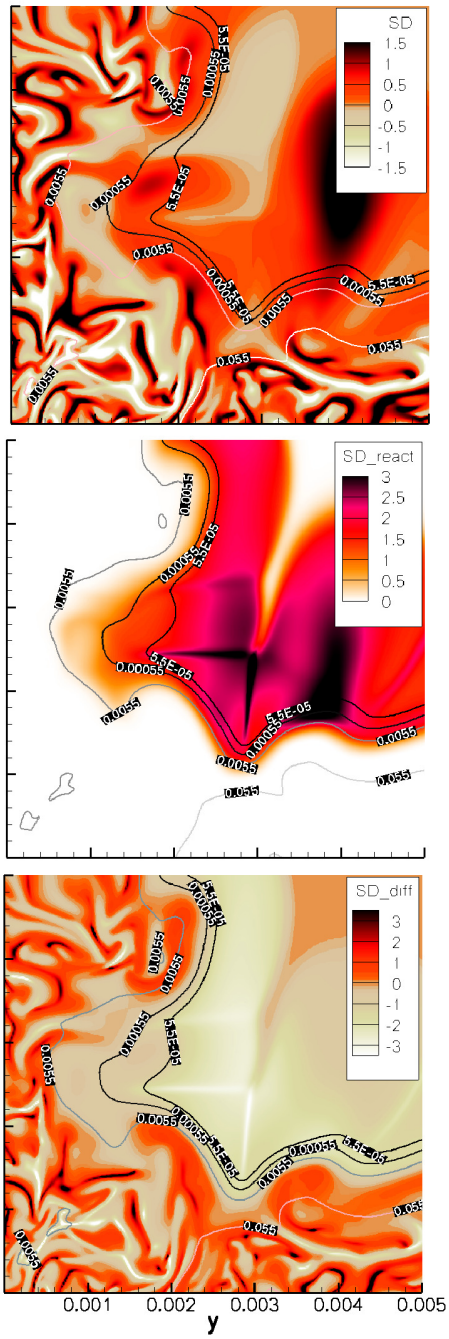

Figure 10: Displacement speed and its components $S_{D,react}$ and $S_{D,diff}$ at time $t/\tau = 1$ with contour lines showing the iso-surfaces of the fuel mass fraction.

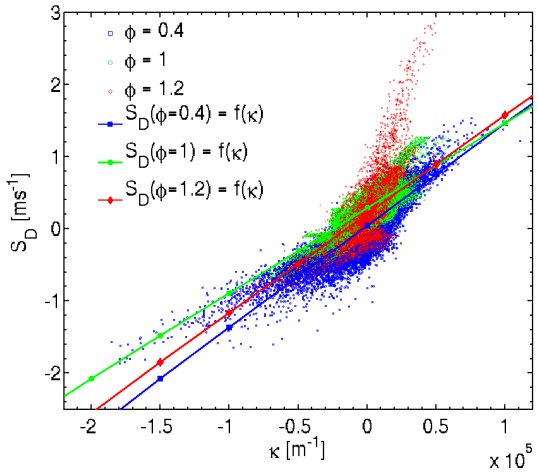

Figure 11: Displacement speed as a function of curvature. Scatter for $t/\tau = 1.5$ with straight lines from the correlation at the initial time.

room temperature cannot sustain a flame. The large amount of flame segments with negative displacement speed results in a lower average S_D in general. The higher displacement speeds in the lean region are due to the support received from the neighbouring flames through diffusive transport of temperature and radicals. The lower speed at rich conditions can be explained by the effect of heat diffusion on flame speed. Due to the stratified nature of this flame, there are temperature gradients along the flame, therefore heat from the points with the highest burning temperature ($\Phi \simeq 1$) is diffused to the surrounding gases. This effectively decreases the temperature at those points and consequently lowers the displacement speed as well. The displacement speeds in the later time steps are consistently lower than those at the initial time and in the laminar case; this is due to heat transfer being enhanced by the wrinkling of the flame turbulent diffusion.

Figs. 10-12 clearly show that there is a large variation in the displacement speed for any given curvature and/or equivalence ratio. This is because the displacement speed in an unsteady three-dimensional flame is highly unsteady as well. To demonstrate this, Fig. 13 shows how S_D varies across a rich part of the flame. S_D varies relatively little inside the reaction zone, while it fluctuates significantly on the unburned side. The preheat zone shows a large variation in S_D due to the small-scale turbulent eddies found there.

The displacement speed varies a lot when viewed in the spatial coordinate x as is done in Fig. 13. However, if the fuel consumption layer is stretched by remapping the flame to fuel mass fraction space a clear plateau emerges. As seen in Fig. 14, this provides a better indication of which value of the fuel mass fraction (and therefore of the progress variable c_1) is appropriate to use to define the displacement speed of the flame.

The displacement speed appears to vary slowly over a larger range in the fuel mass fraction coordinate, which suggests that the choice of iso-surface can be

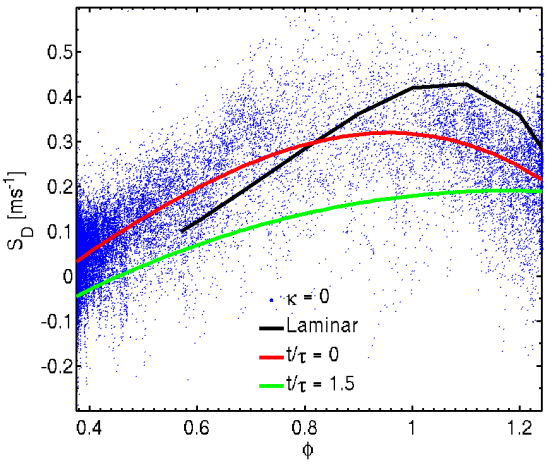

Figure 12: Scatter plot of displacement speed dependence on Φ conditioned at zero curvature (κ). Lines showing the displacement speed for a 1D laminar flame, the best fit line to the initial time points and best fit line of $t/\tau = 1.5$.

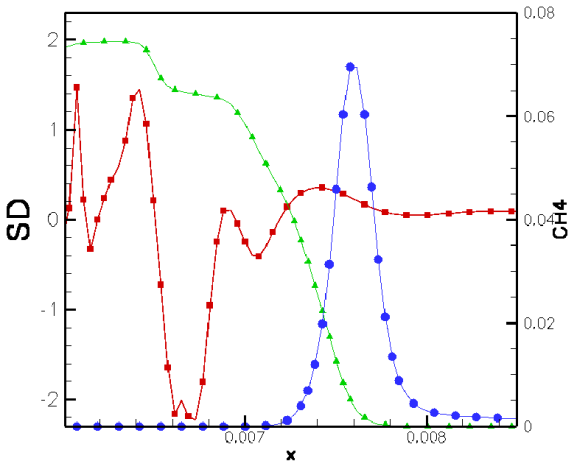

Figure 13: Flame structure for the rich part of the premixed flame at $t/\tau = 1$. The line with squares shows the variation of displacement speed along the flame normal direction. Y_{fuel} (the line with triangles, right axis) and the heat release rate (the line with circles, no axis) are shown to illustrate where the heat release layer is found.

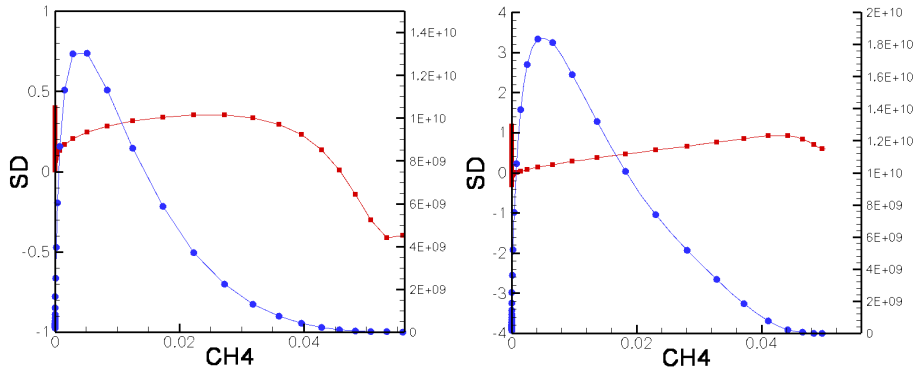

Figure 14: Displacement speed mapped to fuel mass fraction at two different segments of the flame with different equivalence ratios (lines with squares, left $\Phi = 1.2$, right $\Phi = 1$) at $t/\tau = 1$. Heat release rate (lines with circles) is plotted to indicate where the reaction zone is. Points with heat release rate <5e-6 are not plotted.

made by simply choosing the middle of the plateau in the region with high heat release rate. A difficulty remains when discussing partially premixed flames, since the location of this plateau in the fuel mass fraction coordinate is not necessarily the same at all points along the flame, nor can it be assumed that it exists, as can be seen in Fig. 14, right. This is likely a contributing factoer to the large scattering of S_D as shown in Figs. 11 and 12.

In the $\Phi = 1.2$ part of the flame (Fig.14, left) negative displacement speeds are seen to coincide with high fuel mass fraction and low heat release rate. This region corresponds to the preheat zone of the flame. In the stoichiometric part of the flame (Fig. 14, right), S_D is positive in the same region but has rapid small-scale fluctuations where heat release is very low (not shown). The proximity of a diffusion flame behind the flame may be responsible for the distribution of S_D in this part of the flame.

It is important to mention that the displacement speed is calculated based on iso-surfaces of fuel, while a lot of discussion is made in relation to progress variables. For methane fuel mass fraction iso-surfaces are similar to progress variable iso-surfaces, as illustrated in Fig. 15. When discussing hydrogen flames we will see that this approximation becomes highly inappropriate.

4.1.3 Discussion on the modelling of turbulent partially premixed flames

Progress variable and equivalence ratio are commonly used as modelling parameters; therefore, a scatter plot of $c_2 - \Phi$ space at $t/\tau = 1.5$ coloured by heat release is presented in Fig.16. There, it can be seen that there is no unique mapping of heat release rate to $c_2 - \Phi$ space. As the flame is no longer symmetrical at this point we see two areas with high heat release, one at $\Phi = 1$ and one near $\Phi = 1.2$. The heat release rate on the rich side corresponds to the position where the diffusion flame is attached to the premixed front. It is clear that the highest heat release rates, found in the leading premixed flame,

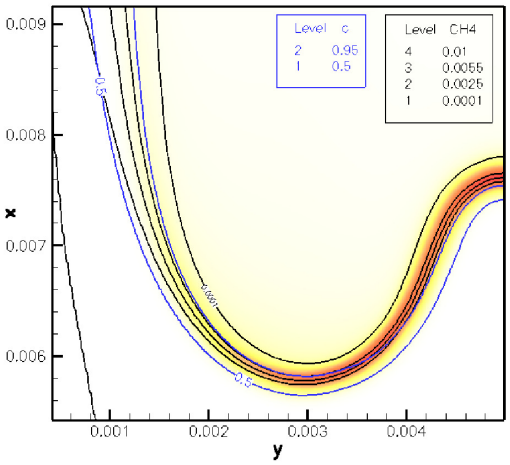

Figure 15: Iso-contours for methane mass fraction, Y_{CH_4}, compared to iso-contours for progress variable. Heat release given as an indication to where the flame is in relation to both.

occur before $c_2 = 0.8$. The low heat release rate at higher c_2 corresponds to the diffusion flame. The lean trail has a low heat release rate sustained until $c_2 \simeq 1$ of comparable magnitude to the diffusion flame.

4.2 Hydrogen/air partially premixed flame

In analogy to the methane flame analysis, the triple flame structures are examined using the equivalence ratio as defined in Eq. (46), and a reaction progress variable.

In hydrogen/air partially premixed flames, due to the high diffusivity of hydrogen, the change of the fuel mass fraction is not only dependent on reaction but also strongly affected by diffusion, especially the additional effect of differential diffusion of hydrogen with respect to other species. Since the normalised fuel mass fraction defined in Eq. (48) accounts for all these effects implicitly some strange results can be obtained in certain conditions. For example, the propagation of an iso-surface of c_1 might not be connected to any reactions. An alternative progress variable, c_3 can be defined based on the product of complete combustion as follows

$$c_3 = Y_{H_2O}/Y^{max}_{H_2O}, \quad Y^{max}_{H_2O} = min(9Y_H, 9Y_O/8), \tag{54}$$

where Y_H and Y_O are the element mass fractions of H and O, respectively.

4.2.1 Structures of hydrogen/air partially premixed flames

Figure 17 shows an instantaneous flame front of the partially premixed hydrogen/air flame defined at $c_1 = 0.4$ at time $t/\tau = 1$, c_1 is defined in Eq. (48). The

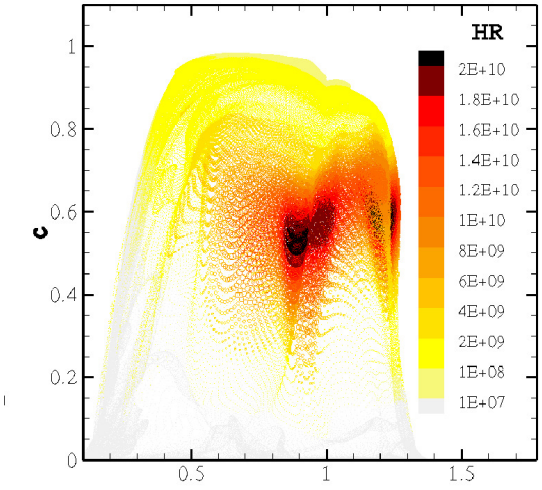

Figure 16: Heat release rate mapped to progress variable c_2 and equivalence ratio Φ.

2D plane shows the distribution of the fuel mass fraction, giving an indication of the position of the diffusion flame.

The flame front is defined at $c_1 = 0.4$ in order to extract both the lean and rich parts of the premixed flame. A very low progress variable value has to be used in this case because, in contrast to the methane flame, the fuel burned in the diffusion flame is the same as that in the premixed flame. This means that the fuel mass fraction in the rich part of the domain does not disappear until after the diffusion flame.

Figure 18 shows the distribution of the reaction progress variable c_1 in the same 2D plane as in Figs. 19 and 20. The gradient of c_1 in the lean part of the premixed flame (close to the lateral boundaries) is so large that the choice of c_1 does not significantly alter the flame position. On the contrary, in the rich part of the flame the gradient of c_1 is quite small. A larger c_1 value is unable to capture the rich premixed flame. For example, if $c_1 = 0.6$ is chosen the flame front extracted is located deep into the burned side of the actual flame. The location of the premixed flame can be easily inferred from the distributions of OH and H radicals in Figs. 19 and 20. Figure 17 shows that the temperature is very low on this surface, especially for the lean part of the flame, which suggests the choice of c_1 is too low to provide an accurate flame surface even in the lean part. The reaction progress variable based on the mass fraction of H_2O defined in Eq. 54 gives a more consistent flame front position with a higher value of c_3.

It is useful to compare the structures of partially premixed flames of different fuels in order to ascertain which characteristics are independent of the specific chemistry details. The partially premixed hydrogen/air flame structure has many similarities to the methane flame studied in the previous section. The most important similarities suggest what can be considered general aspects of partially premixed flames, and are mentioned below.

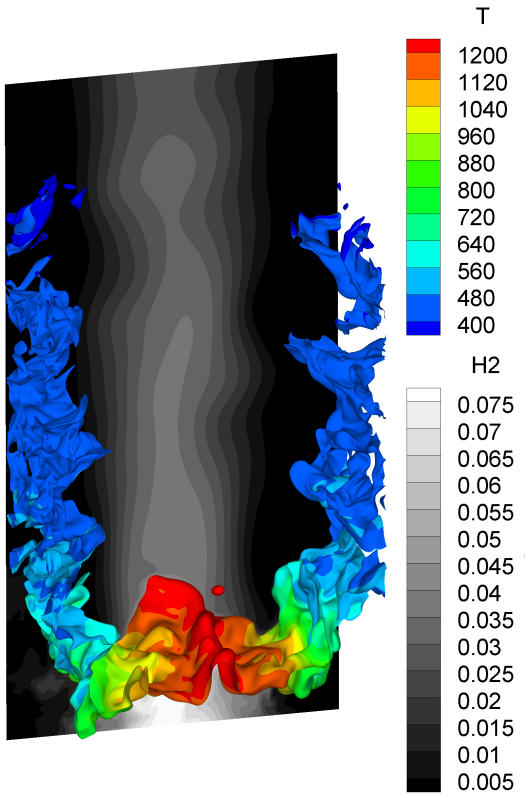

Figure 17: Premixed flame surface coloured with temperature and distribution of H_2 mass fraction in the central plane. The flame surface is defined at $c_1 = 0.4$. Results are taken at $t/\tau = 1$.

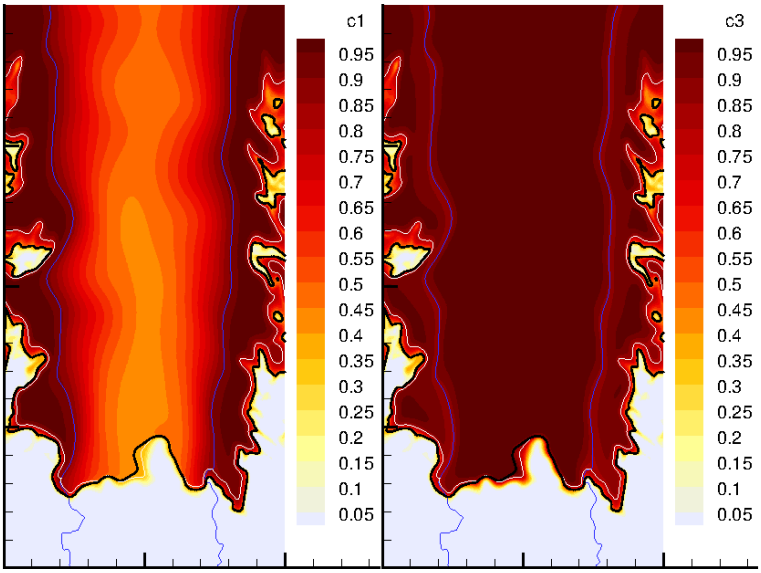

Figure 18: Distributions of the reaction progress variables, (a) c_1 defined in Eq. (48), and (b) c_3 defined in Eq. (54). The solid black line is the iso-contour of $c_1 = 0.4$ in the plane; the white line is the iso-contour of $c_3 = 0.8$; the solid purple line is the iso-contour of $\Phi = 1$ in the plane. Results are taken at $t/\tau = 1$.

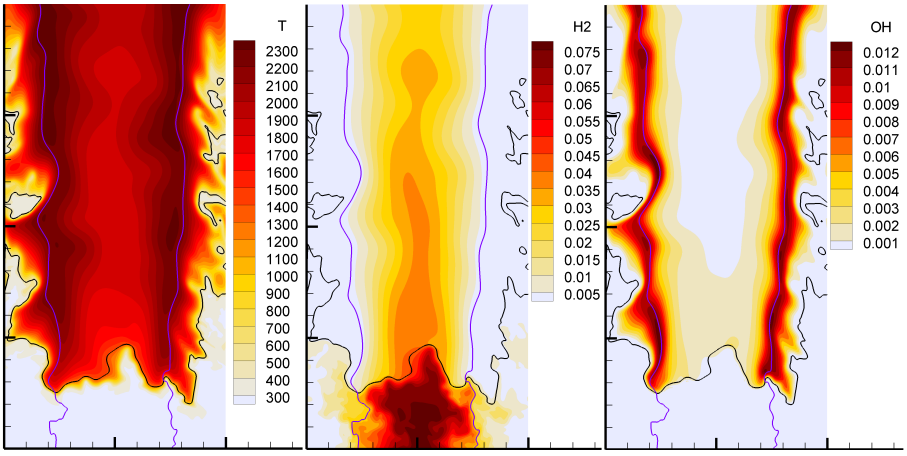

Figure 19: Distribution of temperature, mass fractions of H_2 and OH radicals in the central plane. The solid black line is the iso-contour of $c_1 = 0.4$ in the plane; the solid purple line is the iso-line of $\Phi = 1$ in the plane. Results are taken at $t/\tau = 1$.

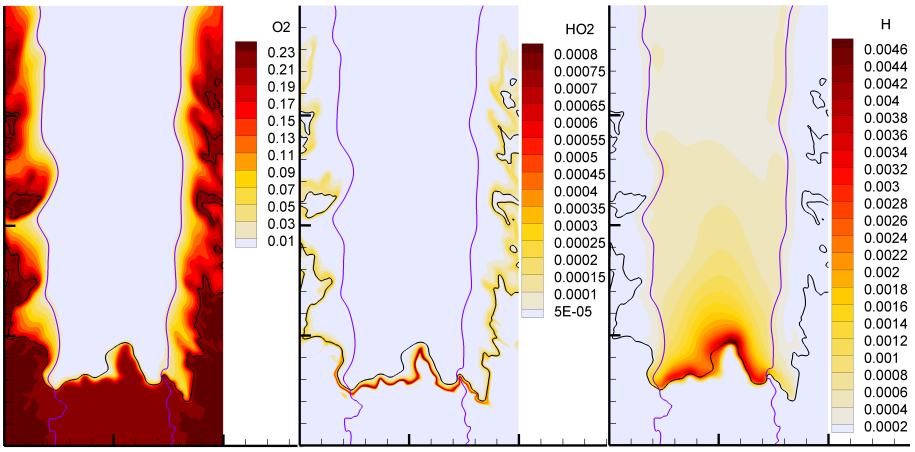

Figure 20: Distribution of mass fractions of O_2, HO_2 and H radicals in the central plane. The solid black line is the iso-contour of $c_1 = 0.4$ in the plane; the solid purple line is the iso-contour of $\Phi = 1$ in the plane.. Results are taken at $t/\tau = 1$.

The triple point of the hydrogen/air partially premixed flame is found around $\Phi = 1$, which is the same as that in the methane/air flame. This is a direct consequence of the definition of triple point, so that in both flames the diffusion flame meets the premixed flame front at $\Phi = 1$. However, what is less self-evident is that the highest displacement speed is found at the triple point for both flames, as is indicated by the W-shape of the flame front. Having the highest propagation speed at $\Phi = 1$ is unsurprising for the methane/air flame, as the laminar flame speed of a methane/air mixture peaks there. However, for hydrogen/air flames the maximum displacement speed is found in a rich mixture, e.g. around $\Phi = 1.8$ [22]. This suggests that the triple flame is in fact enhancing the displacement speed of the stoichiometric mixture in both cases. A possible reason for this effect is the strong influx of OH radicals diffusing from the trailing diffusion flame strengthening heat release reactions, cf. Fig. 19.

Both flames in this study sustain a very lean trailing flame on the edges. The mechanism for supporting the lean trail is the same as for the methane flame: the diffusion of OH radicals generated in the diffusion flame. Due to the periodic boundary conditions the lean premixed flames are very close to each other and at points merge with each other. The species distributions shown in Figs. 19 and 20 suggest that even so the interaction between the neighbouring lean premixed flames is rather weak. The lean hydrogen/air partially premixed flame surface appears to have equivalence ratios as low as 0.1. The lean limit of this flame is quantitatively uncertain as the flame surface is extracted at a very low progress variable value, making it difficult to guarantee the surface is capturing the reaction zone along the entire trail.

The effect of changing fuel results in some distinct differences in the properties of the flames. The first difference that can be easily seen is that the flame front defined by $c_1 = 0.4$ is wrinkled at significantly smaller scales than those found in the methane/air flame. Since the turbulence conditions in the

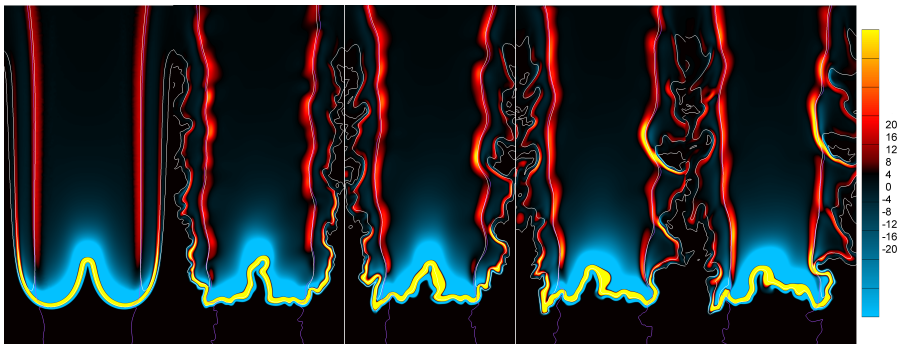

Figure 21: View of the centre plane at different times showing the location of the triple flame visualised with reaction rate of H. From left to right: $t/\tau = 0, 0.5, 1., 1.5, 2.$ where τ is the eddy turnover time. Iso-contours for $c_3 = 0.5$ and $c_3 = 0.93$ are drawn in white. Local equivalence ratio $\Phi = 1$ is shown with a purple line.

two flames are similar, the difference in the wrinkling is likely to be an effect of differential diffusion and thermal-diffusion instability, both characteristic of hydrogen/air flames.

The other difference is that the original fuel is not completely consumed by the premixed flame, as it is in the methane/air flame. In the hydrogen/air flame the diffusion flame burns hydrogen that is found after the premixed front. This difference makes the reaction progress variable based on the fuel mass fraction (c_1) unsuitable for characterising the premixed flame front. For the hydrogen/air partially premixed flame the value of c_1 has to be carefully chosen in order to extract both the lean premixed flame and the rich premixed flame. In terms of modelling the leading premixed flame front, using c_1 can be problematic as the value has to be picked for each case specifically. A possible approach to generalise the choice of c_1 would be to use the local maximum gradient of c_1 to define the flame surface instead of a constant value. Fig. 18 shows that the maximum gradient of c_1 closely matches $c_1 = 0.4$ in this case. Alternatively, using the progress variable c_3 defined in Eq.(54) may be preferable, cf. Fig. 18.

Figure 21 shows 2D distributions of the net reaction rates of H radicals in the hydrogen/air partially premixed flame at different instances of time: from the initial field to the fully developed turbulent flame state.

The formation of H radicals is a result of the elementary reaction OH + H_2 = H + H_2O, where fuel is consumed to form the combustion product, H_2O. The consumption of H radicals is located in the thick layer downstream of premixed front, where H is mainly consumed in the chain branching reaction H + O_2 = O + OH, producing OH radicals. There is also H consumption upstream of the fuel consumption layer. Here the temperature is relatively low and thus the three-body recombination reaction H + O_2 + M = HO_2 + M is important. This low temperature H consumption layer coincides with the HO_2 layer shown in Fig. 20.

In Fig. 21 the reaction progress variable c_3 is shown to coincide very well with the reaction zones. In particular, $c_3 = 0.5$ is suitable for the premixed

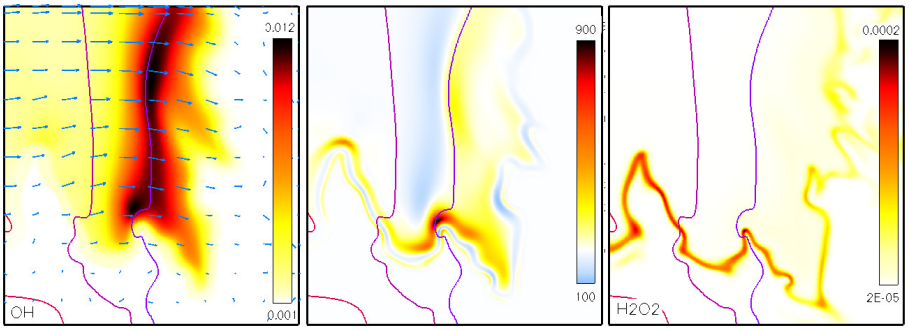

Figure 22: Close-up of the hydrogen flame leading edge showing the distribution of OH (left figure) in relation to the OH reaction rate (middle figure). H_2O_2 (right figure) is used to show the position of the preheat zone. The purple line shows the iso-contour of $\Phi = 1$, while the other lines show iso-contour of $\Phi > 1$.

flame front while $c_3 = 0.93$ coincides well with the lean premixed flame and the diffusion flame. In Fig. 18 the iso-line for $c_3 = 0.8$ is shown to also match the reaction zones well, showing that the product progress variable has a larger range where it fits the flame surfaces.

Figure 22 shows a zoomed region around the triple-point on the bottom right of the leading flame front. As mentioned earlier OH radicals are mainly formed by the chain branching reaction H + O_2 = O + OH; it is highest at the triple-point. The OH consumption is in the fuel-consumption layer. The triple point is shown to be further downstream than rich and lean premixed flame surrounding it. This is an effect of turbulence/flame interaction. The eddies transport OH radicals upstream, resulting in a change of the propagation speed of the reaction front. The effect of eddies on the displacement speed is discussed further in the next section.

4.2.2 Displacement speed of hydrogen/air partially premixed flames

To examine the effect of turbulent eddies on the local displacement speed the distribution of the local displacement speed defined based on the transport equation of fuel mass fraction, Eq. (50), is shown in Fig. 23. Note that the iso-surface of the fuel mass fraction is only an approximation of the iso-surface of the reaction progress variable c_1. Consequently, the displacement speed shown in the figure is also an approximation of the displacement speed of the reaction front.

Figure 23 shows that the displacement speed is strongly correlated to the turbulent eddies. The displacement speed can be both positive (propagating towards the unburned fuel/air) and negative (propagating towards the burned mixture) indicating that the flame is broadening.

The displacement speed in the preheat zone, where fuel mass fraction is high, fluctuates due to the diffusion transport $S_{D,diff}$. This is the result of turbulent eddies in the preheat zone being highly energetic since the local temperature is low enough that the dilation effect is not significant. The eddies move from hot to cold zones and vice versa. This eddy transport has a large effect on the diffusion component of displacement speed and since the reaction contribution

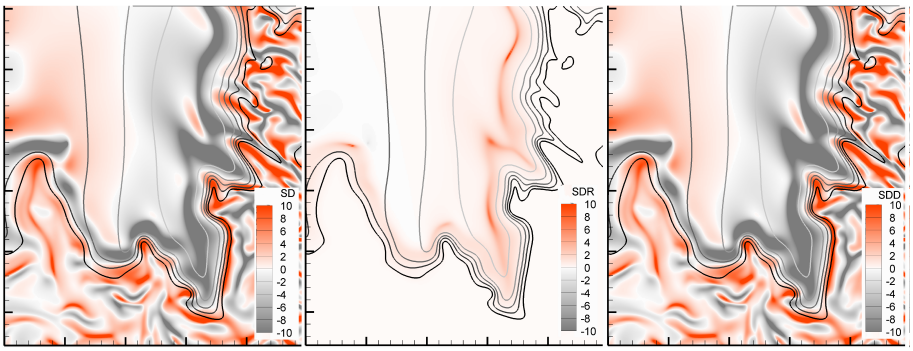

Figure 23: Displacement speed S_D and its components $S_{D,react}$ and $S_{D,diff}$ at time $t/\tau = 1$ with contour lines showing the iso-surfaces of the fuel mass fraction.

is lower in the preheat zone S_D is determined by this term, resulting in negative displacement speeds.

$S_{D,react}$ is always positive and confined to thin layers where the fuel is consumed and heat is released. The local high temperatures resulting from this heat release cause eddy dilation. This is an effect of the gas expansion caused by the low density of hot gases. An eddy that experiences volumetric expansion has lower vorticity and a larger size. This means that the smaller eddies to not survive past the preheat zone.

Figure 24 shows the distribution of the fuel mass fraction, heat release rate and displacement speed across the leading premixed flame at the triple-point. The preheat zone (left to the heat release zone) shows high fluctuations of S_D. The distribution of S_D indicates that different layers of the flame are propagating at different velocities and in different directions. This implies that the structure of the flame evolves with time, locally becoming broader/thinner depending on the flow.

4.2.3 Modelling of hydrogen/air partially premixed flames

From the discussions in the previous sections several observations regarding modelling of hydrogen/air partially premixed flames can be made:

- The choice of progress variable is critical when modelling hydrogen/air turbulent partially premixed flames. As has been stated before, a fuel based progress variable (c_1) is not suitable since the choice of value to define the flame front is problematic. The use of a product based progress variable (c_3) is better, however, it still requires using different values of c_3 to identify all parts of the flame.

- An unsteady flame thickness can cause problems when using flamelet models. The large effect of turbulent eddies on the displacement speed in the preheat zone can cause local broadening and thinning of the flame. Therefore, flamelet models based on stationary flamelet library tabulation can be unsuitable for such flames. The assumption of a flame as a sharp in-

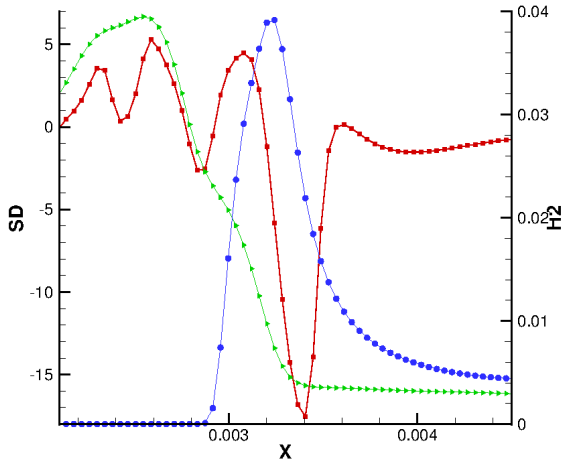

Figure 24: Structure at the triple-point of flame at $t/\tau = 1.5$. The line with squares shows the variation of displacement speed along the flame normal direction. Y_{fuel} (the line with triangles, right axis) and the heat release rate (the line with circles, no axis) are shown to illustrate where the heat release layer is found.

terface can result in non-physical displacement speed fluctuations as the internal structures cannot be captured.

- The local displacement speed is dominated by the effect of turbulent diffusion leading large variations in the speed. There is currently no model that quantifies the correlation between the local turbulent eddies and displacement speed. This poses a great challenge in applying the level-set approach for modelling of turbulent partially premixed flames since the model requires an explicit expression of the local displacement speed as an input to the model.

5 Conclusions and Future Work

Three-dimensional direct numerical simulations are carried out to study the structure of partially premixed methane/air and hydrogen/air flames in turbulent flows. The results are used to improve the understanding of the structures and propagation of turbulent partially premixed flames and to determine the effect of the interaction between the premixed and non-premixed parts of a flame. The following conclusions are drawn.

Structure of partially premixed flames. For both the methane/air flame and the hydrogen/air flame a triple-flame structure is found. The leading premixed flame consists of a lean premixed flame and a rich premixed flame. At the triple-point, which is the point on the leading premixed flame where the mixture is at stoichometry, a diffusion flame trail starts. It is shown that the premixed flame sustains a stable flame at very lean conditions ($\Phi \simeq 0.39$ for the methane/air flame and $\Phi \simeq 0.1$ for the hydrogen/air flame) as a result of support from the neighbouring diffusion flames. The support is primarily due to diffusion of hot combustion products including highly reactive species such as OH radicals. For the methane/air flame the diffusion flame oxidises CO and H_2 formed as intermediates from the rich premixed flame in the leading front. For the hydrogen/air flame the fuel that leaks through the leading premixed flame continues mixing and oxidation in the trail diffusion flame. It is found that the structure of the flame behind the main premixed front is complex, with a range of low-rate reactions taking place in the whole area behind the flame. These reactions are not restricted to the diffusion flame and the lean trailing flame; consequently the diffusion flame cannot be described as a thin sharp reaction zone. Turbulence further aids in mixing, thereby bringing different species in contact with each other. A progress variable based on the products of combustion is shown to be able to capture both the premixed and the diffusion flame surfaces.

Propagation speed of partially premixed flames. It is found that the local displacement speed is highly sensitive to local curvature, equivalence ratio and turbulence conditions. At zero curvature the displacement speed of a turbulent flame is lower than the corresponding laminar ones as well as that of the unstretched planar premixed flame. However, owing to the existence of curvature on the flame front, the displacement speed is in general several times higher than that of the unstretched planar premixed flame. Turbulence appears to have a large effect on the diffusion component of displacement speed, causing a large variation in S_D across the flame as well as along it. That the displacement speed shows such large variation throughout the flame - including segments where it is negative - means that the thickness of the flame is not constant but evolving in time. This aspect of turbulent partially premixed flames differs fundamentally from the laminar flamelet model of premixed flames.

Effect of turbulence on partially premixed flames. It is found that turbulent eddies can enter the preheat zone of the flame under the current high Karlovitz number conditions. The eddies in the preheat zone modify the diffusive transport of heat and mass in the zone, which gives rise to high spatial variation of the local displacement speed, causing highly unsteady thinning and thickening of the flame. Due to changes in curvature and strain rate caused by eddies in the reaction zone, the local reaction rates are highly altered, which further alters the flame structure and displacement speed. In the postflame zone, due to the elevated temperature and the resulting gas expansion, the eddy size increases

and their strength decreases.

The level-set approach was originally developed for flame surface propagation, i.e. infinitely thin flame sheet. It was later extended to thicker flames in the flamelet regime and the thin-reaction zone regime. An underlying assumption of this model is that the time scale of chemistry is faster than the flow time scale so that the flame structure can be assumed to be quasi-steady, i.e., there is no significant temporal evolution of the flame structures. The high sensitivity of local displacement speed to flame curvature, strain rate, equivalence ratio and turbulent eddy motion gives rise to temporally evolving flame structures. Modelling turbulent partially premixed flames using a single level-set formulation is therefore not straightforward. We would like to approach this subject in future work, as effort is needed to accommodate such flame dynamics in the modelling. An attempt using different iso-surfaces in the preheat zone and reaction zone tracked using respective G-equations with locally different displacement speeds and local turbulence field could show how the flame thickness varies with time. The reinitialisation method necessary when working with the G-equation and the signed distance function needs to be revised, and the velocity extension method may be revisited as an alternative.

When using the reaction progress variable and mixture fraction formulation for partially premixed flames, care must be taken when choosing the reaction progress variable. It has been shown that the fuel based progress variable cannot capture the diffusion flame. To develop a computational cost-effective CFD model for partially premixed flames, the mapping of flame structure to the progress variable and other scalars should be investigated further. In the present study it was shown that mapping the flame to progress variable and equivalence ratio space is not sufficient as it cannot uniquely describe the flame.

Acknowledgements

This work was carried out at the division of Fluid Mechanics, department of Energy Sciences, Lund University, Sweden. The work was financially supported by the Swedish Research Council (VR) and the national Centre for Combustion Science and Technology (CeCOST). Computations were performed using computer facilities provided by the Centre for Scientific and Technical Computing at Lund University (LUNARC). I would also like to acknowledge PRACE for awarding access to resources CURIE TN based in France at TGCC.

I would like to start by thanking my supervisor Prof. Xue-Song Bai for having given me the opportunity to start my PhD studies here. Thank you for introducing me to the subject of combustion, and for all the support you provided throughout my studies.

I would also like to thank Dr. Rixin Yu, Dr. Henning Carlsson and Thommie Nilsson for your co-operation in carrying out these studies. Your help has been invaluable, and I thank you for all the discussions and knowledge you have shared with me.

The staff at the division of Fluid Mechanics, and the lovely group of people at the lunch room in the Department of Energy Sciences, deserve my gratitude for having made this a friendly workplace to come to.

My friends and family who have been supportive throughout my studies, and especially Maddy for reading through the entire thesis and giving me comments. And thank you to my cats, for being furry everyday and waking me up at ungodly hours.

Finally I will thank my husband. You have made everything better by being there for me, thank you for all your encouragement and understanding. And for the cats ;)

References

[1] Xue-Song Bai, Michael Balthasar, Fabian Mauss, and Laszlo Fuchs. Detailed soot modeling in turbulent jet diffusion flames. In *Symposium (International) on Combustion*, volume 27, pages 1623–1630. Elsevier, 1998.

[2] Xue-Song Bai, Laszlo Fuchs, and Fabian Mauss. Laminar flamelet structure at low and vanishing scalar dissipation rate. *Combustion and flame*, 120(3):285–300, 2000.

[3] Xue-Song Bai and K Seshadri. Rate-ratio asymptotic analysis of nonpremixed methane flames. *Combustion Theory and Modelling*, 3(1):51–75, 1999.

[4] Eric Baudoin, Xue-Song Bai, Beibei Yan, Changye Liu, R Yu, Andreas Lantz, Seyed Mohammad Hosseini, B Li, A Elbaz, M Sami, et al. Effect of partial premixing on stabilization and local extinction of turbulent methane/air flames. *Flow, turbulence and combustion*, 90(2):269–284, 2013.

[5] Beth Anne V Bennett, Charles S McEnally, Lisa D Pfefferle, and Mitchell D Smooke. Computational and experimental study of axisymmetric coflow partially premixed methane/air flames. *Combustion and Flame*, 123(4):522–546, 2000.

[6] RW Bilger. Turbulent jet diffusion flames. *Progress in Energy and Combustion Science*, 1(2):87–109, 1976.

[7] RW Bilger, SB Pope, KNC Bray, and JF Driscoll. Paradigms in turbulent combustion research. *Proceedings of the Combustion Institute*, 30(1):21–42, 2005.

[8] Roland Borghi. Turbulent combustion modelling. *Progress in Energy and Combustion Science*, 14(4):245–292, 1988.

[9] Ken Bray, Pascale Domingo, and Luc Vervisch. Role of the progress variable in models for partially premixed turbulent combustion. *Combustion and Flame*, 141(4):431–437, 2005.

[10] Peter N Brown, George D Byrne, and Alan C Hindmarsh. Vode: A variable-coefficient ode solver. *SIAM journal on scientific and statistical computing*, 10(5):1038–1051, 1989.

[11] J Buckmaster and M Matalon. Anomalous lewis number effects in tribrachial flames. In *Symposium (International) on Combustion*, volume 22, pages 1527–1535. Elsevier, 1989.

[12] Pierre Cardaliaguet, James Nolen, and Panagiotis E Souganidis. Homogenization and enhancement for the gâequation. *Archive for Rational Mechanics and Analysis*, 199(2):527–561, 2011.

[13] Henning Carlsson, Emil Nordström, Alexis Bohlin, Per Petersson, Yajing Wu, Robert Collin, Marcus Aldén, Per-Erik Bengtsson, and Xue-Song Bai. Large eddy simulations and rotational cars/piv/plif measurements

of a lean premixed low swirl stabilized flame. *Combustion and Flame*, 161(10):2539–2551, 2014.

[14] Henning Carlsson, Emil Nordström, Alexis Bohlin, Yajing Wu, Bo Zhou, Zhongshan Li, Marcus Aldén, Per-Erik Bengtsson, and Xue-Song Bai. Numerical and experimental study of flame propagation and quenching of lean premixed turbulent low swirl flames at different reynolds numbers. *Combustion and Flame*, 162(6):2582–2591, 2015.

[15] Henning Carlsson, Rixin Yu, and Xue-Song Bai. Direct numerical simulation of lean premixed ch 4/air and h 2/air flames at high karlovitz numbers. *International Journal of Hydrogen Energy*, 39(35):20216–20232, 2014.

[16] Henning Carlsson, Rixin Yu, and Xue-Song Bai. Flame structure analysis for categorization of lean premixed ch 4/air and h 2/air flames at high karlovitz numbers: Direct numerical simulation studies. *Proceedings of the Combustion Institute*, 35(2):1425–1432, 2015.

[17] Jacqueline H Chen, Evatt R Hawkes, Ramanan Sankaran, Scott D Mason, and Hong G Im. Direct numerical simulation of ignition front propagation in a constant volume with temperature inhomogeneities: I. fundamental analysis and diagnostics. *Combustion and flame*, 145(1):128–144, 2006.

[18] Jacqueline H Chen and Hong G Im. Correlation of flame speed with stretch in turbulent premixed methane/air flames. In *Symposium (International) on Combustion*, volume 27, pages 819–826. Elsevier, 1998.

[19] Magnus Christensen and Bengt Johansson. Influence of mixture quality on homogeneous charge compression ignition. *SAE Transactions, Journal of Fuels and Lubricants*, 107, 1998.

[20] Michael G Crandall and Pierre-Louis Lions. Viscosity solutions of hamilton-jacobi equations. *Transactions of the American Mathematical Society*, 277(1):1–42, 1983.

[21] Tarek Echekki and Jacqueline H Chen. High-temperature combustion in autoigniting non-homogeneous hydrogen/air mixtures. *Proceedings of the Combustion Institute*, 29(2):2061–2068, 2002.

[22] Irvin Glassman, Richard A Yetter, and Nick G Glumac. *Combustion*. Academic press, 2014.

[23] Jose Gomes and Olivier Faugeras. Reconciling distance functions and level sets. *Journal of Visual Communication and Image Representation*, 11(2):209–223, 2000.

[24] Cheng Gong, Mehdi Jangi, and Xue-Song Bai. Large eddy simulation of n-dodecane spray combustion in a high pressure combustion vessel. *Applied Energy*, 136:373–381, 2014.

[25] L J Hartley and JW Dold. Flame propagation in a nonuniform mixture: analysis of a propagating triple-flame. *Combustion science and technology*, 80(1-3):23–46, 1991.

[26] DC Haworth. Progress in probability density function methods for turbulent reacting flows. *Progress in Energy and Combustion Science*, 36(2):168–259, 2010.

[27] J.O. Hinze. *Turbulence: Second Edition*. McGraw-Hill, 1975.

[28] Hong G Im and Jacqueline H Chen. Structure and propagation of triple flames in partially premixed hydrogen–air mixtures. *Combustion and Flame*, 119(4):436–454, 1999.

[29] Hong G Im and Jacqueline H Chen. Effects of flow strain on triple flame propagation. *Combustion and Flame*, 126(1):1384–1392, 2001.

[30] Mehdi Jangi, Tommaso Lucchini, Gianluca DâErrico, and Xue-Song Bai. Effects of egr on the structure and emissions of diesel combustion. *Proceedings of the Combustion Institute*, 34(2):3091–3098, 2013.

[31] RJ Kee, FM Rupley, JA Miller, ME Coltrin, JF Grcar, E Meeks, HK Moffat, AE Lutz, G Dixon-Lewis, MD Smooke, et al. Chemkin collection, release 3.6, reaction design. *Inc., San Diego, CA*, 2000.

[32] Alan R Kerstein, William T Ashurst, and Forman A Williams. Field equation for interface propagation in an unsteady homogeneous flow field. *Physical Review A*, 37(7):2728, 1988.

[33] PN Kıoni, KNC Bray, DA Greenhalgh, and B Rogg. Experimental and numerical studies of a triple flame. *Combustion and Flame*, 116(1):192–206, 1999.

[34] PN Kioni, B Rogg, KNC Bray, and A Linán. Flame spread in laminar mixing layers: the triple flame. *Combustion and Flame*, 95(3):276–290, 1993.

[35] YS Ko and SH Chung. Propagation of unsteady tribrachial flames in laminar non-premixed jets. *Combustion and Flame*, 118(1):151–163, 1999.

[36] Andrey Nikolaevich Kolmogorov. The local structure of turbulence in incompressible viscous fluid for very large reynolds numbers. In *Dokl. Akad. Nauk SSSR*, volume 30, pages 299–303, 1941.

[37] Song-Charng Kong, Zhiyu Han, and Rolf D Reitz. The development and application of a diesel ignition and combustion model for multidimensional engine simulation. Technical report, SAE Technical Paper, 1995.

[38] Robert H Kraichnan. Diffusion by a random velocity field. *Physics of Fluids (1958-1988)*, 13(1):22–31, 1970.

[39] BJ Lee and SH Chung. Stabilization of lifted tribrachial flames in a laminar nonpremixed jet. *Combustion and Flame*, 109(1):163–172, 1997.

[40] Bo Li, Eric Baudoin, Rixin Yu, ZW Sun, ZS Li, Xue-Song Bai, Marcus Alden, and MS Mansour. Experimental and numerical study of a conical turbulent partially premixed flame. *Proceedings of the Combustion Institute*, 32(2):1811–1818, 2009.

[41] Juan Li, Zhenwei Zhao, Andrei Kazakov, and Frederick L Dryer. An updated comprehensive kinetic model of hydrogen combustion. *International journal of chemical kinetics*, 36(10):566–575, 2004.

[42] ZS Li, Bo Li, ZW Sun, Xue-Song Bai, and Marcus Aldén. Turbulence and combustion interaction: high resolution local flame front structure visualization using simultaneous single-shot plif imaging of ch, oh, and ch 2 o in a piloted premixed jet flame. *Combustion and Flame*, 157(6):1087–1096, 2010.

[43] Sung King Liew, KNC Bray, and JB Moss. A flamelet model of turbulent non-premixed combustion. *Combustion Science and Technology*, 27(1-2):69–73, 1981.

[44] Andrei N Lipatnikov and Vladimir A Sabel'nikov. Some basic issues of the averaged g-equation approach to premixed turbulent combustion modeling. *Open Thermodynamics Journal*, 2:53–58, 2008.

[45] Changye Liu, Beibei Yan, G Chen, and Xue-Song Bai. Structures and burning velocity of biomass derived gas flames. *International Journal of hydrogen energy*, 35(2):542–555, 2010.

[46] Yu-Yu Liu, Jack Xin, and Yifeng Yu. A numerical study of turbulent flame speeds of curvature and strain g-equations in cellular flows. *Physica D: Nonlinear Phenomena*, 243(1):20–31, 2013.

[47] Bjørn F Magnussen and Bjørn H Hjertager. On mathematical modeling of turbulent combustion with special emphasis on soot formation and combustion. In *Symposium (International) on Combustion*, volume 16, pages 719–729. Elsevier, 1977.

[48] E Mallard and H Le Chatelier. Combustion of explosive gas mixtures. *Ann. Mines*, 8:274, 1883.

[49] Vincent Moureau, Benoit Fiorina, and Heinz Pitsch. A level set formulation for premixed combustion les considering the turbulent flame structure. *Combustion and Flame*, 156(4):801–812, 2009.

[50] K-J Nogenmyr, C Fureby, Xue-Song Bai, P Petersson, Robert Collin, and Mark Linne. Large eddy simulation and laser diagnostic studies on a low swirl stratified premixed flame. *Combustion and Flame*, 156(1):25–36, 2009.

[51] K-J Nogenmyr, Per Petersson, Xue-Song Bai, Christer Fureby, Robert Collin, Andreas Lantz, Mark Linne, and Marcus Alden. Structure and stabilization mechanism of a stratified premixed low swirl flame. *Proceedings of the Combustion Institute*, 33(1):1567–1574, 2011.

[52] K-J Nogenmyr, Per Petersson, Xue-Song Bai, A Nauert, Jimmy Olofsson, C Brackman, Hans Seyfried, Johan Zetterberg, ZS Li, Mattias Richter, et al. Large eddy simulation and experiments of stratified lean premixed methane/air turbulent flames. *Proceedings of the Combustion Institute*, 31(1):1467–1475, 2007.

[53] Karl-Johan Nogenmyr, J Kiefer, ZS Li, Xue-Song Bai, and Marcus Aldén. Numerical computations and optical diagnostics of unsteady partially premixed methane/air flames. *Combustion and flame*, 157(5):915–924, 2010.

[54] James Nolen and Alexei Novikov. Homogenization of the g-equation with incompressible random drift in two dimensions. *arXiv preprint arXiv:1011.0016*, 2010.

[55] Martin Oberlack and Alexei F Cheviakov. Higher-order symmetries and conservation laws of the g-equation for premixed combustion and resulting numerical schemes. *Journal of Engineering Mathematics*, 66(1-3):121–140, 2010.

[56] Martin Oberlack, Holger Wenzel, and Norbert Peters. On symmetries and averaging of the g-equation for premixed combustion. *Combustion Theory and Modelling*, 5(3):363–383, 2001.

[57] Rebecca Owston and John Abraham. Structure of hydrogen triple flames and premixed flames compared. *Combustion and Flame*, 157(8):1552–1565, 2010.

[58] Norbert Peters. Laminar diffusion flamelet models in non-premixed turbulent combustion. *Progress in energy and combustion science*, 10(3):319–339, 1984.

[59] Norbert Peters. *Turbulent combustion*. Cambridge university press, 2000.

[60] Norbert Peters and Forman A Williams. Liftoff characteristics of turbulent jet diffusion flames. *AIAA journal*, 21(3):423–429, 1983.

[61] H Pitsch. A consistent level set formulation for large-eddy simulation of premixed turbulent combustion. *Combustion and Flame*, 143(4):587–598, 2005.

[62] H Pitsch and N Peters. A consistent flamelet formulation for non-premixed combustion considering differential diffusion effects. *Combustion and Flame*, 114(1):26–40, 1998.

[63] H Pitsch and H Steiner. Large-eddy simulation of a turbulent piloted methane/air diffusion flame (sandia flame d). *Physics of Fluids (1994-present)*, 12(10):2541–2554, 2000.

[64] Tobias Plessing, Peter Terhoeven, Norbert Peters, and Mohy S Mansour. An experimental and numerical study of a laminar triple flame. *Combustion and Flame*, 115(3):335–353, 1998.

[65] SB Pope. Pdf methods for turbulent reactive flows. *Progress in Energy and Combustion Science*, 11(2):119–192, 1985.

[66] Lewis F Richardson. Some measurements of atmospheric turbulence. *Philosophical Transactions of the Royal Society of London. Series A, Containing Papers of a Mathematical or Physical Character*, pages 1–28, 1921.

[67] V Sabel'nikov, A Yu Ovsyannikov, and M Gorokhovski. Modified level set equation for gas-liquid interfaces and its numerical solution. In *Proceedings of 6th European Congress on Computational Methods in Applied Sciences and Engineering, ECCOMAS*, volume 2012, pages 5597–5611, 2012.

[68] Vladimir Sabelnikov and Christer Fureby. Les combustion modeling for high re flames using a multi-phase analogy. *Combustion and Flame*, 160(1):83–96, 2013.

[69] Vladimir Sabel'nikov and Andrei Lipatnikov. Rigorous derivation of an unclosed mean g-equation for statistically 1d premixed turbulent flames. *International Journal of Spray and Combustion Dynamics*, 2(4):301–323, 2010.

[70] K Seshadri. Multistep asymptotic analyses of flame structures. In *Symposium (International) on Combustion*, volume 26, pages 831–846. Elsevier, 1996.

[71] K Seshadri, Xue-Song Bai, H Pitsch, and N Peters. Asymptotic analysis of the structure of moderately rich methane-air flames. *Combustion and flame*, 113(4):589–602, 1998.

[72] K Seshadri and N Peters. The inner structure of methane/air flames. *Combustion and Flame*, 81(2):96–118, 1990.

[73] K Seshadri, N Peters, and FA Williams. Asymptotic analyses of stoichiometric and lean hydrogen-air flames. *Combustion and Flame*, 96(4):407–427, 1994.

[74] Ko Seshadri and N Peters. Asymptotic structure and extinction of methaneî¸ air diffusion flames. *Combustion and Flame*, 73(1):23–44, 1988.

[75] James Albert Sethian. *Level set methods and fast marching methods: evolving interfaces in computational geometry, fluid mechanics, computer vision, and materials science*, volume 3. Cambridge university press, 1999.

[76] GI Sivashinsky. Diffusional-thermal theory of cellular flames. *Combustion Science and Technology*, 15(3-4):137–145, 1977.

[77] Johan Sjöholm, Joakim Rosell, Bo Li, Mattias Richter, Zhongshan Li, Xue-Song Bai, and Marcus Aldén. Simultaneous visualization of oh, ch, ch 2 o and toluene plif in a methane jet flame with varying degrees of turbulence. *Proceedings of the Combustion Institute*, 34(1):1475–1482, 2013.

[78] Mitchell D Smooke. Reduced kinetic mechanisms and asymptotic approximations for methane-air flames: a topical volume. In *Reduced Kinetic Mechanisms and Asymptotic Approximations for Methane-Air Flames*, volume 384, 1991.

[79] Rickard Solsjö, Mehdi Jangi, Clement Chartier, Öivind Andersson, and X-S Bai. Lift-off and stabilization of n-heptane combustion in a diesel engine with a multiple-nozzle injection. *Proceedings of the Combustion Institute*, 34(2):3031–3038, 2013.

[80] MB Sun, ZG Wang, and Xue-Song Bai. Assessment and modification of sub-cell-fix method for re-initialization of level-set distance function. *International journal for numerical methods in fluids*, 62(2):211–236, 2010.

[81] Mark Sussman, Peter Smereka, and Stanley Osher. A level set approach for computing solutions to incompressible two-phase flow. *Journal of Computational physics*, 114(1):146–159, 1994.

[82] Hendrik Tennekes and John Leask Lumley. *A first course in turbulence*. MIT press, 1972.

[83] Stephen R Turns et al. *An introduction to combustion*, volume 287. McGraw-hill New York, 1996.

[84] JA Van Oijen and LPH De Goey. A numerical study of confined triple flames using a flamelet-generated manifold. *Combustion Theory and Modelling*, 8(1):141–164, 2004.

[85] F.A. Williams. *Combustion Theory*. Westview Press, 1994.

[86] Jack Xin, Yifeng Yu, et al. Periodic homogenization of the inviscid g-equation for incompressible flows. *Communications in Mathematical Sciences*, 8(4):1067–1078, 2010.

[87] Murat Yaldizli, Kian Mehravaran, Hyderuddin Mohammad, and Farhad A Jaberi. The structure of partially premixed methane flames in high-intensity turbulent flows. *Combustion and Flame*, 154(4):692–714, 2008.

[88] Beibei Yan, Bo Li, Eric Baudoin, Changye Liu, ZW Sun, ZS Li, Xue-Song Bai, Marcus Aldén, G Chen, and MS Mansour. Structures and stabilization of low calorific value gas turbulent partially premixed flames in a conical burner. *Experimental Thermal and Fluid Science*, 34(3):412–419, 2010.

[89] Mingfa Yao, Zhaolei Zheng, and Haifeng Liu. Progress and recent trends in homogeneous charge compression ignition (hcci) engines. *Progress in Energy and Combustion Science*, 35(5):398–437, 2009.

[90] JF Yu, Rixin Yu, XQ Fan, Moah Christensen, AA Konnov, and Xue-Song Bai. Onset of cellular flame instability in adiabatic ch 4/o 2/co 2 and ch 4/air laminar premixed flames stabilized on a flat-flame burner. *Combustion and Flame*, 160(7):1276–1286, 2013.

[91] Rixin Yu and Xue-Song Bai. Direct numerical simulation of lean hydrogen/air auto-ignition in a constant volume enclosure. *Combustion and Flame*, 160(9):1706–1716, 2013.

[92] Rixin Yu and Xue-Song Bai. A semi-implicit scheme for large eddy simulation of piston engine flow and combustion. *International Journal for Numerical Methods in Fluids*, 71(1):13–40, 2013.

[93] Rixin Yu and Xue-Song Bai. A fully divergence-free method for generation of inhomogeneous and anisotropic turbulence with large spatial variation. *Journal of Computational Physics*, 256:234–253, 2014.

[94] Rixin Yu, Jiangfei Yu, and Xue-Song Bai. An improved high-order scheme for dns of low mach number turbulent reacting flows based on stiff chemistry solver. *Journal of Computational Physics*, 231(16):5504–5521, 2012.

[95] IA Zeldovich, G Io Barenblatt, VB Librovich, and GM Makhviladze. Mathematical theory of combustion and explosions. 1985.

[96] Ya B Zeldovich. Regime classification of an exothermic reaction with nonuniform initial conditions. *Combustion and Flame*, 39(2):211–214, 1980.

[97] Fan Zhang, JF Yu, Rixin Yu, Mehdi Jangi, and Xue-Song Bai. Dns of co/h2/air ignition in a constant volume enclosure relevant to direct injection hcci engine. In *7th Mediterranean Combustion Symposium, MCS7*, 2011.

[98] Fan Zhang, Rixin Yu, and Xue-Song Bai. Detailed numerical simulation of syngas combustion under partially premixed combustion engine conditions. *International Journal of Hydrogen Energy*, 37(22):17285–17293, 2012.

[99] Y Zhang, B Rogg, and KNC Bray. 2-d simulation of turbulent autoignition with transient laminar flamelet source term closure. *Combustion science and technology*, 105(4-6):211–227, 1995.

[100] Bo Zhou, Christian Brackmann, Qing Li, Zhenkan Wang, Per Petersson, Zhongshan Li, Marcus Aldén, and Xue-song Bai. Distributed reactions in highly turbulent premixed methane/air flames: Part i. flame structure characterization. *Combustion and Flame*, 2015.

[101] Bo Zhou, Christian Brackmann, Zhongshan Li, Marcus Aldén, and Xue-Song Bai. Simultaneous multi-species and temperature visualization of premixed flames in the distributed reaction zone regime. *Proceedings of the Combustion Institute*, 35(2):1409–1416, 2015.